Computational Materials Science 83 (2014) 235–249

Contents lists available at ScienceDirect

Computational Materials Science

journal homepage: www.elsevier.com/locate/commatsci

Trefftz-Lekhnitskii Grains (TLGs) for efficient Direct Numerical Simulation (DNS) of the micro/meso mechanics of porous piezoelectric materials

Peter L. Bishay [a,*], Satya N. Atluri [a,b]

[a] International Collaboratory for Fundamental Studies in the Engineering Sciences (ICES), University of California, Irvine, CA, USA
[b] Multidisciplinary Engineering & Computer Science, King Abdulaziz University, Jeddah, Saudi Arabia

ARTICLE INFO

Article history:
Received 21 July 2013
Accepted 27 October 2013

Keywords:
Piezoelectric
Porous
Trefftz
Lekhnitskii
Voronoi cells
Void

ABSTRACT

We consider a class of piezoelectric materials with defects, voids, and/or elastic dielectric or piezoelectric inclusions. We develop computationally highly efficient as well as mathematically highly accurate methods for the Direct Numerical Simulation (DNS) of micro/meso mechanics of such materials, for the purposes of: 1. determining the meso/macro physical properties of such materials, and 2. studying the mechanics of damage initiation at the micro-level in such materials. In this paper, we develop what we label as "Trefftz-Lekhnitskii Grains (TLGs)", each of which can model a single grain of piezoelectric materials with voids. These TLGs are of arbitrary geometrical shapes, to mimic the natural shape of each micro-grain of the material.

The TLGs are based on expressing the mechanical and electrical fields in the interior of each grain in terms of the Trefftz solution functions derived from Lekhnitskii formulation for piezoelectric materials. The potential functions are written in terms of Laurent series which can describe interior or exterior domains where negative exponents are used only in the latter case. The boundary conditions at the outer boundaries of each TLG can be enforced using a boundary variational principle, collocation or least squares method, while the boundary conditions at the inner (void/inclusion) boundary can be enforced using collocation/least squares, or by using the *special solution set* which satisfy the traction-free, charge-free boundary conditions at the void periphery. These various methods of enforcing the boundary conditions generate different grains which are denoted as TLG-BVPs, TLG-C, TLG-Cs, TLG-LS, TLG-LSs (where BVP refers to "boundary variational principle", C refers to "collocation", LS refers to "Least Squares", and s refers to "special solution set"). Several examples of the DNS of micro/meso mechanics of porous piezoelectric materials are presented, not only to determine the macro physical properties of such materials, but also to study the mechanisms for damage precursors in such intelligent materials.

1. Introductions and literature review

Piezoelectric materials are smart materials that are strained when subjected to electric fields (this is the so-called "direct effect") and are electrically polarized when they are strained (which is the "converse effect"). During the last 4 decades, large amounts of experimental, analytical and computational research were conducted to study the linear and non-linear behaviors of such materials in different applications under different loading conditions. Transducers, actuators, frequency generators and smart material systems for aerospace and medical industries, are among the several applications of these materials.

Piezoelectric ceramics are also used in smart composite materials because these composites possess some enhanced properties over monolithic piezoelectric materials such as bigger range of coupled properties, better acoustic properties or figures of merit, and less brittleness. Both "subtractive" and "additive" approaches were used to develop piezoelectric composites where, in the "subtractive" approach, controlled porosity are added to the piezoelectric material to form porous piezoelectric material with reduced density [1]. These porous piezoelectric materials found applications such as miniature accelerometers, vibration sensors, contact microphones and hydrophones. On the other hand, in the "additive" approach, the effective properties of the composite are optimized by combining two or more constituents. The second phase could be dielectric ceramic [2], metal [3], or polymer [4] to modulate the electrical properties. Piezoelectric ceramics are also used in smart composite materials where piezoelectric rods (fibers) are embedded in an elastic matrix.

Porous piezoelectric materials have several advantages such as lack of possibility of destructive chemical reactions between the

* Corresponding author. Tel.: +1 (949) 351 3412; fax: +1 (949) 824 9967.
E-mail address: bishayp@uci.edu (P.L. Bishay).

0927-0256/$ - see front matter © 2013 Elsevier B.V. All rights reserved.
http://dx.doi.org/10.1016/j.commatsci.2013.10.038

piezoelectric ceramic and the second phase during production (porous piezoelectric ceramics are composed of ceramics only, the second phase is air), ability to control pore size, shape and distribution (hence piezoelectric properties can be tailored), light weight compared to monolithic piezoelectric materials and piezoelectric composites, reduced price of production compared to other piezoelectric composites, and low acoustic impedances compared to dense ceramics, hence they could be used to improve the mismatch of acoustic impedances at the interfaces of medical ultrasonic imaging devices or underwater sonar detectors [5].

Analytical models of porous piezoelectric materials are only available for simple geometries such as infinite plate with circular or elliptical holes as presented in [6–9] using either Lekhnitskii formalism [10] or the extended Stroh formalism [11]. However for more complicated geometries and practical problems, numerical methods such as finite elements, boundary elements, meshless or Trefftz methods should be used.

Modeling domains with defects (holes, inclusions or cracks) using the ordinary finite element method needs mesh refinement around defects in order to achieve acceptable results for the gradients of fields; hence it is very complex, time-consuming, and costly. Thus, special methods should be used to model defects. Special methods for Direct Numerical Simulation (DNS) of micro/meso structures of isotropic elastic materials were developed by Dong and Atluri as 2D and 3D Trefftz [12–14] and SGBEM cells [15–18], where each cell models an entire grain of the material, with elastic/rigid inclusions or voids, for direct numerical micromechanical analysis of composite and porous materials. Elements with elliptical holes were also developed by Wang and Qin [19]. For piezoelectric materials, Wang et al. [20] developed a hybrid finite element with a hole based on Lekhnitskii formalism, while Cao et al. [21] developed a hybrid finite element with defects based on the extended Stroh formalism. The boundary element method was also used by Xu and Rajapakse [22] to analyze piezoelectric materials with elliptical holes. In addition, Trefftz Cells were used to model microstructures with defects, using the multi-source-point Trefftz method in [23] for plane elasticity, and multi-domain Trefftz boundary collocation method for plane piezoelectricity macromechanics developed by Sheng et al. [24] based on Lekhnitskii formalism.

The basic idea of the various Trefftz methods is to use the so-called Trefftz functions which satisfy the homogenous governing equations of the relevant physical phenomenon as the trial and/or weight functions. A complete set of Trefftz functions that satisfy only the homogenous governing equations is sometimes termed as a *basic solution set*. A complete set of Trefftz functions that satisfy both the homogenous governing equations and the homogenous boundary conditions is sometimes termed as a *special solution set*. To formulate any Trefftz methods, Trefftz functions must be available.

In this paper, Trefftz-Lekhnitskii Grains (TLGs) are developed for modeling porous piezoelectric materials where each grain has an arbitrarily polygonal shape, and may or may not include a circular or an arbitrarily oriented elliptical void, for Direct Numerical Simulation of the micromechanics of porous piezoelectric materials. The advantage of using TLGs is that each TLG may represent a single grain in the material that has its own polling direction. The Dirichlet tessellation used to construct the mesh and the geometric shapes of the TLGs resembles the physical configurations of the grains in the mesomechanics, wherein each grain may be surrounded by an arbitrary number of neighboring grains; hence TLGs are expected to show field distributions that cannot be obtained using regular triangular and four-sided elements. Lekhnitskii formalism is employed here due to the relatively explicit nature of the derived Trefftz functions. 2D and 3D radial basis function (RBF) grains and SGBEM grains were successfully used to model the switching phenomena in ferroelectric materials by Bishay and Atluri [25] and to model heterogeneous and functionally graded materials in [26,27,12–18].

For TLGs that include voids, three methods can be used to enforce matrix boundary primal fields' continuity. These methods are boundary variational principle (BVP), collocation (C), or least squares (LS), while void boundary conditions can be enforced using collocation/least squares method or by using the special solution set which is available only for impermeable voids. Accordingly, five types of grains are presented here and denoted as TLG-C, TLG-LS, TLG-BVPs, TLG-Cs and TLG-LSs (where the last "s" in the latter three denotes "special solution set"). There is no need to enforce void boundary conditions in the latter three grains, because the special solution set already satisfies the traction-free, charge-free conditions. This makes these grains more efficient. However, for other cases, such as grains with piezoelectric or dielectric inclusions, the special solution set does not exist and hence it is very important to present the first two grain types which will be extended to the aforementioned cases in a future work.

The paper is organized as follows: Section 2 introduces all governing equations and boundary conditions. Lekhnitskii's solution for plane piezoelectric problem is presented in Section 3, while Trefftz-Lekhnitskii Grain (TLG) formulation for piezoelectric materials with/without voids is introduced in Section 4. Numerical examples are provided in Section 5 and conclusions are summarized in Section 6.

2. Governing equations and boundary conditions

Consider a domain Ω filled with piezoelectric material or porous piezoelectric material. On the boundary of the domain, denoted $\partial\Omega$, we can specify displacement on S_u or traction on S_t (not both at any point. i.e., $S_u \cap S_t = \emptyset$). Similarly we can specify electric potential on S_φ or electric charge per unit area (electric displacement) on S_Q (where again $S_\varphi \cap S_Q = \emptyset$). So $\partial\Omega = S_u \cup S_t = S_\varphi \cup S_Q$. The whole domain Ω can be divided into N elements $\Omega = \sum_{e=1}^{N} \Omega^e$ (where each element may represent a grain in the material). The intersection of the boundary of grain e, denoted $\partial\Omega^e$, with S_u, S_t, S_φ and S_Q is S_u^e, S_t^e, S_φ^e and S_Q^e, while the intersection with the neighboring grain boundaries is denoted S_g^e. Hence $\partial\Omega^e = S_u^e \cup S_t^e \cup S_g^e = S_\varphi^e \cup S_Q^e \cup S_g^e$.

Each grain domain, Ω^e, may contain a void filling the domain Ω_c^e and has a boundary $\partial\Omega_c^e$ such that $\Omega_c^e \subset \Omega^e$ and $\partial\Omega_c^e \cap \partial\Omega^e = \emptyset$. In this case, the region outside the void domain in grain e is called the matrix domain $\Omega_m^e = \Omega^e - \Omega_c^e$. Fig. 1 (left) shows one grain (irregular polygonal element in the 2D case) with an arbitrary void. The figure also shows the crystallographic coordinates and the polling direction.

Adopting matrix and vector notation and denoting $\mathbf{u}$ (2 components), $\boldsymbol{\varepsilon}$ (3 components) and $\boldsymbol{\sigma}$ (3 components) as the mechanical displacement vector, strain and stress tensors written in vector form respectively, and φ (scalar), $\mathbf{E}$ (2 components) and $\mathbf{D}$ (2 components) as the electric potential, electric field and electric displacement vectors respectively. The following equations should be satisfied in the piezoelectric matrix domain, Ω_m^e:

(1) Stress equilibrium and Charge conservation (Gauss's) equations:

$$\partial_{\mathbf{u}}^T \boldsymbol{\sigma} + \bar{\mathbf{b}} = \mathbf{0}; \quad \boldsymbol{\sigma} = (\boldsymbol{\sigma})^T, \quad \partial_{\mathbf{e}}^T \mathbf{D} - \bar{\rho}_f = 0 \tag{1}$$

where $\bar{\mathbf{b}}$ is the body force vector, and $\bar{\rho}_f$ is the electric free charge density (which is approximately zero for dielectric and piezoelectric materials).

(2) Strain–displacement and Electric field–electric potential equations:

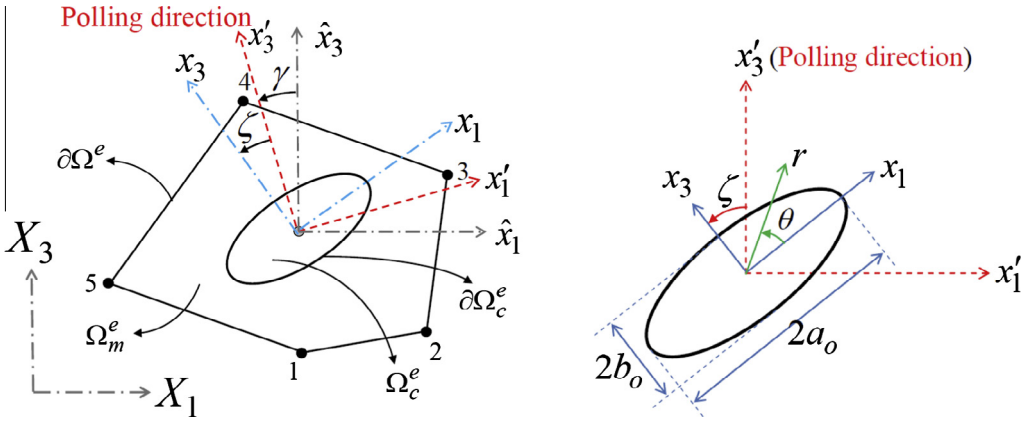

Fig. 1. (left) 2D irregular polygon (grain) with an elliptical void and its local coordinates $(x_1 - x_3)$ as well as the global $(X_1 - X_3)$, grain local $(\hat{x}_1 - \hat{x}_3)$ and crystallographic $(x_1' - x_3')$ Cartesian coordinate systems, (right) Elliptical void and its local coordinate system as well as the polling direction of the piezoelectric material.

$$\boldsymbol{\varepsilon} = \partial_{\mathbf{u}}\mathbf{u}, \quad \mathbf{E} = -\partial_{\mathbf{e}}\varphi \tag{2}$$

where $\partial_{\mathbf{u}} = \begin{bmatrix} \frac{\partial}{\partial x_1} & 0 & \frac{\partial}{\partial x_3} \\ 0 & \frac{\partial}{\partial x_3} & \frac{\partial}{\partial x_1} \end{bmatrix}^T \quad \partial_{\mathbf{e}} = \begin{bmatrix} \frac{\partial}{\partial x_1} & \frac{\partial}{\partial x_3} \end{bmatrix}^T$

This representation of electric field (Eq. (2)), as gradients of an electric potential includes the assumption that Faraday's equation ($\nabla \times \mathbf{E} = -\frac{\partial \mathbf{B}}{\partial t} = \mathbf{0}$, where $\mathbf{B}$ is the magnetic flux density) is satisfied for electrostatics. Note that we consider only two equations (Gauss's and Faraday's equations) from the four Maxwell's equations. The remaining two equations (Gauss's law for magnetism and Ampere's law with Maxwell's correction) are not considered in the electrostatic analysis of piezoelectric materials.

(3) Piezoelectric material constitutive laws:

$$\begin{aligned} \boldsymbol{\sigma} &= \mathbf{C}_{\mathbf{E}}\boldsymbol{\varepsilon} - \mathbf{e}^T\mathbf{E} \\ \mathbf{D} &= \mathbf{e}\boldsymbol{\varepsilon} + \mathbf{h}_{\boldsymbol{\varepsilon}}\mathbf{E} \end{aligned} \quad \text{or} \quad \begin{aligned} \boldsymbol{\varepsilon} &= \mathbf{S}_{\mathbf{D}}\boldsymbol{\sigma} + \mathbf{g}^T\mathbf{D} \\ \mathbf{E} &= -\mathbf{g}\boldsymbol{\sigma} + \boldsymbol{\beta}_{\boldsymbol{\sigma}}\mathbf{D} \end{aligned} \tag{3}$$

where $\mathbf{C}_{\mathbf{E}}$, $\mathbf{h}_{\boldsymbol{\varepsilon}}$, $\mathbf{S}_{\mathbf{D}}$, $\boldsymbol{\beta}_{\boldsymbol{\sigma}}$ are, respectively, the elastic stiffness tensor measured under constant electric field, dielectric permittivity tensor measured under constant strain, elastic compliance tensor measured under constant electric displacement, and inverse of the dielectric permittivity tensor measured under constant stress. $\mathbf{e}$ and $\mathbf{g}$ are piezoelectric tensors measured under constant strain and stress respectively.
The SI units of the mentioned fields are as follows: stress $\boldsymbol{\sigma}$ (Pa or N/m^2), strain $\boldsymbol{\varepsilon}$ (m/m), electric displacement $\mathbf{D}$ (C/m^2), electric field $\mathbf{E}$ (V/m or N/C), and the SI units of the material matrices are: $\mathbf{C}_{\mathbf{E}}$ (Pa or N/m^2), $\mathbf{S}_{\mathbf{D}}$ (m^2/N), $\mathbf{h}_{\boldsymbol{\varepsilon}}$ (C/Vm), $\boldsymbol{\beta}_{\boldsymbol{\sigma}}$ (Vm/C), $\mathbf{e}$ (C/m^2), and $\mathbf{g}$ (m^2/C).
Note that $\mathbf{S}_{\mathbf{D}} \neq (\mathbf{C}_{\mathbf{E}})^{-1}$ and $\boldsymbol{\beta}_{\boldsymbol{\sigma}} \neq (\mathbf{h}_{\boldsymbol{\varepsilon}})^{-1}$. The material constants in Eq. (3) are related through:

$$\begin{bmatrix} \mathbf{S}_{\mathbf{D}} & \mathbf{g}^T \\ -\mathbf{g} & \boldsymbol{\beta}_{\boldsymbol{\sigma}} \end{bmatrix} = \begin{bmatrix} \mathbf{C}_{\mathbf{E}} & -\mathbf{e}^T \\ \mathbf{e} & \mathbf{h}_{\boldsymbol{\varepsilon}} \end{bmatrix}^{-1} \tag{4}$$

Matrix boundary conditions:

(1) Mechanical natural (traction) and essential (displacement) boundary conditions:

$$\mathbf{n}_{\boldsymbol{\sigma}}\boldsymbol{\sigma} = \bar{\mathbf{t}} \quad \text{at } S_t \text{ or } S_t^e, \quad \mathbf{u} = \bar{\mathbf{u}} \quad \text{at } S_u \text{ or } S_u^e, \tag{5}$$

(2) Electric natural and essential boundary conditions:

$$\mathbf{n}_{\mathbf{e}}\mathbf{D} = \overline{Q} \quad \text{at } S_Q \text{ or } S_Q^e, \quad \varphi = \bar{\varphi} \quad \text{at } S_\varphi \text{ or } S_\varphi^e, \tag{6}$$

$$\text{where} \quad \mathbf{n}_{\boldsymbol{\sigma}} = \begin{bmatrix} n_1 & 0 & n_3 \\ 0 & n_3 & n_1 \end{bmatrix}, \quad \text{and} \quad \mathbf{n}_{\mathbf{e}} = [\,n_1 \quad n_3\,], \tag{7}$$

$\bar{\mathbf{t}}$ is the specified boundary traction vector, $\overline{Q}$ is the specified surface density of free charge. n_1 and n_3, the two components present in $\mathbf{n}_{\boldsymbol{\sigma}}$ and $\mathbf{n}_{\mathbf{e}}$ are the components of the unit outward normal to the boundaries S_t (or S_t^e), and S_Q (or S_Q^e), respectively. $\bar{\mathbf{u}}$ is the specified mechanical displacement vector at the boundary S_u (or S_u^e), $\bar{\varphi}$ is the specified electric potential at the boundary S_φ (or S_φ^e).

The following conditions should also be satisfied at each inter-grain boundary S_g^e:

(1) Mechanical displacement and Electric potential compatibility conditions:

$$\mathbf{u}^+ = \mathbf{u}^-, \quad \varphi^+ = \varphi^- \tag{8}$$

(2) Mechanical traction and Electric charge reciprocity conditions:

$$(\mathbf{n}_{\boldsymbol{\sigma}}\boldsymbol{\sigma})^+ + (\mathbf{n}_{\boldsymbol{\sigma}}\boldsymbol{\sigma})^- = 0, \quad (\mathbf{n}_{\mathbf{e}}\mathbf{D})^+ + (\mathbf{n}_{\mathbf{e}}\mathbf{D})^- = 0 \tag{9}$$

Impermeable void boundary conditions

Dielectric constants of piezoelectric materials are three orders of magnitude higher than that of air or vacuum inside the void. This means that charges do not accumulate on the void boundary and the impermeable assumption can be adopted. We then have *traction-free, charge-free* conditions along the void boundary, $\partial\Omega_c^e$:

$$\mathbf{t} = \mathbf{n}_{\boldsymbol{\sigma}}\boldsymbol{\sigma} = \mathbf{0}, \quad Q = \mathbf{n}_{\mathbf{e}}\mathbf{D} = 0 \tag{10}$$

2.1. Plane-stress and plane-strain assumptions

If the considered body is very thin in the 2-direction (plane stress case), the assumptions: $\sigma_2' = \sigma_4' = \sigma_6' = 0$, $D_2' = 0$ can be used and the constitutive equation (Eq. (3)) of a piezoelectric material polled in the crystal axis 3, with respect to the crystallographic axes $x_1' - x_3'$ can be written as:

$$\begin{Bmatrix} \varepsilon_1' \\ \varepsilon_3' \\ \varepsilon_5' \\ E_1' \\ E_3' \end{Bmatrix} = \begin{bmatrix} S_{11}' & S_{13}' & 0 & 0 & g_{31}' \\ S_{13}' & S_{33}' & 0 & 0 & g_{33}' \\ 0 & 0 & S_{44}' & g_{15}' & 0 \\ 0 & 0 & -g_{15}' & \beta_{11}' & 0 \\ -g_{31}' & -g_{33}' & 0 & 0 & \beta_{33}' \end{bmatrix} \begin{Bmatrix} \sigma_1' \\ \sigma_3' \\ \sigma_5' \\ D_1' \\ D_3' \end{Bmatrix} \tag{11}$$

where subscripts of material matrices in Eq. (3) are omitted for simplicity.

If the body is very long (infinite) in the 2-direction (plane strain case), then we have the assumptions: $\varepsilon'_2 = \varepsilon'_4 = \varepsilon'_6 = 0,\ E'_2 = 0$, and the constitutive equation can be written as:

$$\begin{Bmatrix} \varepsilon'_1 \\ \varepsilon'_3 \\ \varepsilon'_5 \\ E'_1 \\ E'_3 \end{Bmatrix} = \begin{bmatrix} \bar{S}'_{11} & \bar{S}'_{13} & 0 & 0 & \bar{g}'_{31} \\ \bar{S}'_{13} & \bar{S}'_{33} & 0 & 0 & \bar{g}'_{33} \\ 0 & 0 & \bar{S}'_{44} & \bar{g}'_{15} & 0 \\ 0 & 0 & -\bar{g}'_{15} & \bar{\beta}'_{11} & 0 \\ -\bar{g}'_{31} & -\bar{g}'_{33} & 0 & 0 & \bar{\beta}'_{33} \end{bmatrix} \begin{Bmatrix} \sigma'_1 \\ \sigma'_3 \\ \sigma'_5 \\ D'_1 \\ D'_3 \end{Bmatrix} \tag{12}$$

where

$$\bar{S}'_{11} = \frac{S'^2_{11} - S'^2_{12}}{S'_{11}}, \quad \bar{S}'_{13} = \frac{S'_{13}(S'_{11} - S'_{12})}{S'_{11}}, \quad \bar{S}'_{33} = \frac{S'_{11}S'_{33} - S'^2_{13}}{S'_{11}},$$
$$\bar{S}'_{44} = S'_{44}$$
$$\bar{g}'_{31} = \frac{g'_{31}(S'_{11} - S'_{12})}{S'_{11}}, \quad \bar{g}'_{33} = \frac{S'_{11}g'_{33} - S'_{13}g'_{31}}{S'_{11}}, \quad \bar{g}'_{15} = g'_{15},$$
$$\bar{\beta}'_{11} = \beta'_{11}, \quad \bar{\beta}'_{33} = \frac{S'_{11}\beta'_{33} + g'^2_{31}}{S'_{11}}$$

3. General solution of plane piezoelectricity using Lekhnitskii formulation

Let (x'_1, x'_3) be the principal material (crystallographic) coordinates, x'_3 be the poling direction and (x_1, x_3) be the set of coordinates obtained by rotating (x'_1, x'_3) through an anti-clockwise rotation ζ, see Fig. 1(right). Using Lekhnitskii formalism, Xu and Rajapakse [7] derived the general solution of plane piezoelectricity with respect to (x_1, x_3) coordinate system as follows:

The constitutive equation with respect to the crystallographic axes $x'_1 - x'_3$ for plane stress and plane strain problems, with the stress and electric displacement as the objectives of the equations, can be written in compact form as:

$$\begin{Bmatrix} \boldsymbol{\varepsilon}' \\ \mathbf{E}' \end{Bmatrix} = \begin{bmatrix} \mathbf{S}' & \mathbf{g}'^T \\ -\mathbf{g}' & \boldsymbol{\beta}' \end{bmatrix} \begin{Bmatrix} \boldsymbol{\sigma}' \\ \mathbf{D}' \end{Bmatrix} \tag{13}$$

where subscripts of material matrices in Eq. (3) are omitted for simplicity.

By invoking tensor transformation rule, the constitutive relations can be written with respect to (x_1, x_3) coordinate system as:

$$\begin{Bmatrix} \varepsilon_1 \\ \varepsilon_3 \\ \varepsilon_5 \\ E_1 \\ E_3 \end{Bmatrix} = \begin{bmatrix} S_{11} & S_{13} & S_{15} & g_{11} & g_{31} \\ S_{13} & S_{33} & S_{35} & g_{13} & g_{33} \\ S_{15} & S_{35} & S_{55} & g_{15} & g_{35} \\ -g_{11} & -g_{13} & -g_{15} & \beta_{11} & \beta_{13} \\ -g_{31} & -g_{33} & -g_{35} & \beta_{13} & \beta_{33} \end{bmatrix} \begin{Bmatrix} \sigma_1 \\ \sigma_3 \\ \sigma_5 \\ D_1 \\ D_3 \end{Bmatrix} \text{ or } \begin{Bmatrix} \boldsymbol{\varepsilon} \\ \mathbf{E} \end{Bmatrix} = \begin{bmatrix} \mathbf{S} & \mathbf{g}^T \\ -\mathbf{g} & \boldsymbol{\beta} \end{bmatrix} \begin{Bmatrix} \boldsymbol{\sigma} \\ \mathbf{D} \end{Bmatrix} \tag{14}$$

In which

$$\mathbf{S} = \mathbf{T}_2^T \mathbf{S}' \mathbf{T}_2, \quad \mathbf{g} = \mathbf{T}_1^T \mathbf{g}' \mathbf{T}_2, \quad \boldsymbol{\beta} = \mathbf{T}_1^T \boldsymbol{\beta}' \mathbf{T}_1 \tag{15}$$

In the above equations,

$$\mathbf{T_1} = \begin{bmatrix} \cos\zeta & -\sin\zeta \\ \sin\zeta & \cos\zeta \end{bmatrix} \text{ and}$$
$$\mathbf{T_2} = \begin{bmatrix} \cos^2\zeta & \sin^2\zeta & -2\sin\zeta\cos\zeta \\ \sin^2\zeta & \cos^2\zeta & 2\sin\zeta\cos\zeta \\ \sin\zeta\cos\zeta & -\sin\zeta\cos\zeta & \cos^2\zeta - \sin^2\zeta \end{bmatrix}.$$

It can be seen that the coefficients $\mathbf{S}$, $\mathbf{g}$ and $\boldsymbol{\beta}$ are functions of the angular rotation ζ.

Based on Lekhnitskii formalism, two complex potential functions: stress function, $\phi(x_1, x_3)$, and induction function, $\psi(x_1, x_3)$, are introduced as:

$$\sigma_1 = \frac{\partial^2\phi(x_1,x_3)}{\partial x_3^2}, \quad \sigma_3 = \frac{\partial^2\phi(x_1,x_3)}{\partial x_1^2}, \quad \sigma_5 = -\frac{\partial^2\phi(x_1,x_3)}{\partial x_1 \partial x_3},$$
$$D_1 = \frac{\partial\psi(x_1,x_3)}{\partial x_3}, \quad D_3 = -\frac{\partial\psi(x_1,x_3)}{\partial x_1}. \tag{16}$$

The balance rules for plane piezoelectricity (Eq. (1)) in the absence of body force and free-charge density ($\bar{\mathbf{b}} = \mathbf{0}$, $\overline{\rho_f} = 0$) can be satisfied by Eq. (16). Substituting Eq. (16) into Eq. (14) and invoking the following strain and electric field compatibility equations:

$$\frac{\partial^2\varepsilon_1}{\partial x_3^2} + \frac{\partial^2\varepsilon_3}{\partial x_1^2} - \frac{\partial^2\varepsilon_5}{\partial x_1 \partial x_3} = 0, \quad \frac{\partial E_1}{\partial x_1} - \frac{\partial E_3}{\partial x_3} = 0 \tag{17}$$

two differential equations coupled in $\phi(x_1, x_3)$ and $\psi(x_1, x_3)$ can be obtained. Eliminating $\psi(x_1, x_3)$, the governing equations of plane piezoelectricity are reduced to the following sixth-order differential equation which can be written symbolically as:

$$F_1F_2F_3F_4F_5F_6\phi(x_1,x_3) = 0 \tag{18}$$

where $F_k = (\partial/\partial x_3) - \mu_k(\partial/\partial x_1)$ and μ_k ($k = 1, \ldots, 6$) are the roots of the characteristic equation:

$$c_6\mu^6 + c_5\mu^5 + c_4\mu^4 + c_3\mu^3 + c_2\mu^2 + c_1\mu + c_0 = 0. \tag{19}$$

where

$$c_0 = S_{33}\beta_{33} + g_{33}^2, \quad c_1 = -2S_{35}\beta_{33} - 2S_{33}\beta_{13} - 2g_{33}(g_{13} + g_{35}),$$
$$c_2 = S_{33}\beta_{11} + 4S_{35}\beta_{13} + \beta_{33}(2S_{13} + S_{55}) + 2g_{33}(g_{31} + g_{15}) + (g_{13} + g_{35})^2,$$
$$c_3 = -2g_{11}g_{33} - 2S_{15}\beta_{33} - 2S_{35}\beta_{11} - 2\beta_{13}(2S_{13} + S_{55}) - 2(g_{31} + g_{15})(g_{13} + g_{35}),$$
$$c_4 = S_{11}\beta_{33} + 4S_{15}\beta_{13} + \beta_{11}(2S_{13} + S_{55}) + 2g_{11}(g_{13} + g_{35}) + (g_{31} + g_{15})^2,$$
$$c_5 = -2S_{11}\beta_{13} - 2S_{15}\beta_{11} - 2g_{11}(g_{31} + g_{15}), \quad c_6 = S_{11}\beta_{11} + g_{11}^2.$$

In general, the roots of Eq. (19) are complex with three conjugate pairs, i.e.

$$\mu_1 = A_1 + iB_1, \quad \mu_2 = A_2 + iB_2, \quad \mu_3 = A_3 + iB_3,$$
$$\mu_4 = \bar{\mu}_1, \quad \mu_5 = \bar{\mu}_2, \quad \mu_6 = \bar{\mu}_3 \tag{20}$$

in which $i = \sqrt{-1}$, A_k and B_k ($k = 1, 2, 3$) are all distinct. Over-bar denotes complex conjugate. Integration of Eq. (18) leads to the general solution for the complex potential function $\phi(x_1, x_3)$ as:

$$\phi(x_1, x_3) = 2\mathrm{Re}\sum_{k=1}^{3}\phi_k(z_k) \tag{21}$$

where $\phi_k(z_k)$ is an arbitrary function of the complex variable $z_k = x_1 + \mu_k x_3$. Introducing three new complex potential functions:

$$\omega_k(z_k) = \frac{\partial\phi_k(z_k)}{\partial z_k}, \quad k = 1, 2, 3, \tag{22}$$

the stress, electric displacement, strain and electric field components can be expressed in terms of the complex potential functions $\omega_k(z_k)$ as:

$$\begin{Bmatrix} \sigma_1 \\ \sigma_3 \\ \sigma_5 \end{Bmatrix} = 2\mathrm{Re}\sum_{k=1}^{3}\begin{Bmatrix} \mu_k^2 \\ 1 \\ -\mu_k \end{Bmatrix}\omega'_k(z_k), \quad \begin{Bmatrix} D_1 \\ D_3 \end{Bmatrix} = 2\mathrm{Re}\sum_{k=1}^{3}\begin{Bmatrix} \delta_k\mu_k \\ -\delta_k \end{Bmatrix}\omega'_k(z_k)$$
$$\begin{Bmatrix} \varepsilon_1 \\ \varepsilon_3 \\ \varepsilon_5 \end{Bmatrix} = 2\mathrm{Re}\sum_{k=1}^{3}\begin{Bmatrix} p_k \\ q_k \\ r_k \end{Bmatrix}\omega'_k(z_k), \quad \begin{Bmatrix} E_1 \\ E_3 \end{Bmatrix} = -2\mathrm{Re}\sum_{k=1}^{3}\begin{Bmatrix} s_k \\ t_k \end{Bmatrix}\omega'_k(z_k) \tag{23}$$

where the prime ($'$) denotes derivative with respect to z_k and,

$$\delta_k = \frac{g_{11}\mu_k^3 - (g_{15}+g_{31})\mu_k^2 + (g_{13}+g_{35})\mu_k - g_{33}}{\beta_{11}\mu_k^2 - 2\beta_{13}\mu_k + \beta_{33}},$$
$$p_k = S_{11}\mu_k^2 + S_{13} - S_{15}\mu_k + \delta_k(g_{11}\mu_k - g_{31}),$$
$$q_k = S_{13}\mu_k^2 + S_{33} - S_{35}\mu_k + \delta_k(g_{13}\mu_k - g_{33}),$$
$$r_k = S_{15}\mu_k^2 + S_{35} - S_{55}\mu_k + \delta_k(g_{15}\mu_k - g_{35}),$$
$$s_k = g_{11}\mu_k^2 + g_{13} - g_{15}\mu_k - \delta_k(\beta_{11}\mu_k - \beta_{13}),$$
$$t_k = g_{31}\mu_k^2 + g_{33} - g_{35}\mu_k - \delta_k(\beta_{13}\mu_k - \beta_{33}).$$

Invoking the gradient relations for plane piezoelectricity in Eq. (2), the general solution for displacement and electric potential can be obtained as:

$$\begin{Bmatrix} u_1 \\ u_3 \\ \varphi \end{Bmatrix} = 2\mathrm{Re}\sum_{k=1}^{3} \begin{Bmatrix} p_k \\ q_k/\mu_k \\ s_k \end{Bmatrix} \omega_k(z_k) \tag{24}$$

3.1. Basic solution sets

For an elliptical void as shown in Fig. 1(right), the following conformal mapping can be used to transform an ellipse in z_k-plane into a unit circle in ξ_k-plane [28]:

$$z_k = \frac{a_o - i\mu_k b_o}{2}\xi_k + \frac{a_o + i\mu_k b_o}{2}\xi_k^{-1}, \quad k = 1,2,3 \tag{25}$$

where a_o and b_o are the half lengths of the void axes as shown in Fig. 1(right). The inverse mapping has the form:

$$\xi_k = \frac{z_k \pm \sqrt{z_k^2 - \left(a_o^2 + \mu_k^2 b_o^2\right)}}{a_o - i\mu_k b_o}, \quad k = 1,2,3 \tag{26}$$

where the sign of the square root (±) is chosen in such a way that $|\xi_k| \geqslant 1$.

Using the general solution, the plane piezoelectric problem has been reduced to the one of solving for the complex potential functions ω_k. For interior domain problems without flux singularities, ω_k can be represented by Taylor series [29], i.e.

$$\omega_k(z_k) = \sum_{n=0}^{\infty}\left(a_k^{(n)} + ib_k^{(n)}\right)z_k^n, \quad k = 1,2,3 \tag{27}$$

In the case of a domain exterior to an elliptical void, ω_k can be represented by Laurent series in terms of ξ_k instead of z_k [29].

$$\omega_k(\xi_k) = \sum_{n=0}^{\infty}\left(a_k^{(n)} + ib_k^{(n)}\right)\xi_k^n + \sum_{n=1}^{\infty}\left(a_k^{(-n)} + ib_k^{(-n)}\right)\xi_k^{-n}, \quad k = 1,2,3 \tag{28}$$

where $a_k^{(\pm n)}$ and $b_k^{(\pm n)}$ (k = 1, 2, 3 and n = 1, 2, 3, ...) are real coefficients. Along the void boundary which is a unit circle in the ξ_k-plane, we have: $|\xi_k| = 1$ or $\xi_1 = \xi_2 = \xi_3 = e^{i\Theta}$ where $\Theta \in [-\pi, \pi]$. Note that $\bar{\xi}_k^n = \xi_k^{-n}$ on the unit circle.

For exterior domains, $\omega_k(z_k)$ and $\omega_k'(z_k)$ are replaced by $\omega_k(\xi_k)$ and $\frac{\omega_k'(\xi_k)}{z_k'(\xi_k)}$ in Eqs. (23) and (24), where $z_k' = A - B\xi_k^{-2}$, $A = \frac{a_o - i\mu_k b_o}{2}$; $B = \frac{a_o + i\mu_k b_o}{2}$ and the prime (′) now denotes derivative with respect to ξ_k. Hence, in the coming equations, the following will be used:

$$Z_k = \begin{cases} z_k & \text{for interior domains} \\ \xi_k & \text{for exterior domains} \end{cases}$$
$$Y_k^{n-1} = \begin{cases} z_k^{n-1} & \text{for interior domains} \\ \frac{\xi_k^{n-1}}{A - B\xi_k^{-2}} & \text{for exterior domains} \end{cases}$$

By substituting ω_k in Eq. (27), or Eq. (28) into Eq. (24), the *basic set* of Trefftz functions for electromechanical displacement $\underline{\mathbf{u}} = \{u_1, u_3, \varphi\}^T$, electromechanical stress and strain $\boldsymbol{\sigma} = \{\sigma_1 \;\; \sigma_3 \;\; \sigma_5 \;\; D_1 \;\; D_3\}^T$, $\boldsymbol{\varepsilon} = \{\varepsilon_1 \;\; \varepsilon_3 \;\; \varepsilon_5 \;\; E_1 \;\; E_3\}^T$ for interior or exterior domain problems respectively, can be obtained as:

$$\underline{\mathbf{u}} = 2\sum_{n=M_s}^{M}\sum_{k=1}^{3}\Big[\left(\mathrm{Re}(\mathcal{D}_k)\mathrm{Re}(Z_k^n) - \mathrm{Im}(\mathcal{D}_k)\mathrm{Im}(Z_k^n)\right)a_k^{(n)} - \left(\mathrm{Re}(\mathcal{D}_k)\mathrm{Im}(Z_k^n) + \mathrm{Im}(\mathcal{D}_k)\mathrm{Re}(Z_k^n)\right)b_k^{(n)}\Big] \tag{29}$$

$$\underline{\boldsymbol{\sigma}} = 2\sum_{n=M_s}^{M}\sum_{k=1}^{3}\Big[\left(\mathrm{Re}(\mathcal{G}_k)\mathrm{Re}\left(nY_k^{n-1}\right) - \mathrm{Im}(\mathcal{G}_k)\mathrm{Im}\left(nY_k^{n-1}\right)\right)a_k^{(n)} - \left(\mathrm{Re}(\mathcal{G}_k)\mathrm{Im}\left(nY_k^{n-1}\right) + \mathrm{Im}(\mathcal{G}_k)\mathrm{Re}\left(nY_k^{n-1}\right)\right)b_k^{(n)}\Big] \tag{30}$$

$$\underline{\boldsymbol{\varepsilon}} = 2\sum_{n=M_s}^{M}\sum_{k=1}^{3}\Big[\left(\mathrm{Re}(\mathcal{H}_k)\mathrm{Re}\left(nY_k^{n-1}\right) - \mathrm{Im}(\mathcal{H}_k)\mathrm{Im}\left(nY_k^{n-1}\right)\right)a_k^{(n)} - \left(\mathrm{Re}(\mathcal{H}_k)\mathrm{Im}\left(nY_k^{n-1}\right) + \mathrm{Im}(\mathcal{H}_k)\mathrm{Re}\left(nY_k^{n-1}\right)\right)b_k^{(n)}\Big] \tag{31}$$

In the above, $\mathcal{D}_k = \{p_k, q_k/\mu_k, s_k\}^T$, $\mathcal{G}_k = \{\mu_k^2, 1, -\mu_k, \delta_k\mu_k, -\delta_k\}^T$, $\mathcal{H}_k = \{p_k, q_k, r_k, -s_k, -t_k\}^T$ and the upper limit of n (the maximum order of Z_k used in Trefftz functions) is taken to be M for numerical implementation, while the lower limit M_s is taken as:

$$M_s = \begin{cases} 0 & \text{for interior domains} \\ -M & \text{for exterior domains} \end{cases}$$

For interior/exterior solutions, when n is increased by one, six/twelve Trefftz functions with their corresponding undetermined real coefficients $\left\{a_1^{(\pm n)}, b_1^{(\pm n)}, a_2^{(\pm n)}, b_2^{(\pm n)}, a_3^{(\pm n)}, b_3^{(\pm n)}\right\}$ are added to the solution. So the number of Trefftz functions m_T (which is also equivalent to the number of undetermined real coefficients) is:

$$m_T = \begin{cases} 6(M+1) & \text{for interior domain solution} \\ 6(2M+1) & \text{for exterior domain solution} \end{cases} \tag{32}$$

Note that when n = 0, the associated six Trefftz functions correspond to rigid-body modes (constant mechanical displacements and electric potential), and vanishing stress, strain, electric field and electric displacement: $\underline{\boldsymbol{\sigma}} = \mathbf{0}$, $\underline{\boldsymbol{\varepsilon}} = \mathbf{0}$, $\underline{\mathbf{u}} = 2\sum_{k=1}^{3}\left[\mathrm{Re}(\mathcal{D}_k)a_k^{(0)} - Im(\mathcal{D}_k)b_k^{(0)}\right]$.

Generally speaking, it is impossible to find a closed form solution for $\omega_k(\xi_k)$ for arbitrary boundary conditions. For the case of impermeable elliptical void, a special solution set can be found as will be presented in the next subsection.

3.2. Special solution set for impermeable elliptical void

Trefftz special solution set accounts for the homogeneous boundary conditions of voids, cracks etc. Wang et al. [20] constructed a special solution set of Trefftz functions for elliptical voids with axes parallel/perpendicular to polling direction. Sheng et al. [24] extended this to the case of an arbitrarily oriented impermeable elliptical voids.

Note that generally along any boundary surface, we can write [6]:

$$\psi = 2\mathrm{Re}\sum_{k=1}^{3}\delta_k\omega_k(z_k) = -\int_0^s (D_3 n_3 + D_1 n_1)ds = -\int_0^s Q ds$$
$$\frac{\partial\phi(x_1,x_3)}{\partial x_3} = 2\mathrm{Re}\sum_{k=1}^{3}\mu_k\omega_k(z_k) = \int_0^s (n_1\sigma_1 + n_3\sigma_5)ds = \int_0^s t_1 ds$$
$$\frac{\partial\phi(x_1,x_3)}{\partial x_1} = 2\mathrm{Re}\sum_{k=1}^{3}\omega_k(z_k) = -\int_0^s (n_1\sigma_5 + n_3\sigma_3)ds = -\int_0^s t_3 ds \tag{33}$$

So for traction-free, charge-free boundary conditions along the void surface, the following conditions should be satisfied:

$$\mathrm{Re}\sum_{k=1}^{3}\omega_k(\xi_k)=0,\quad \mathrm{Re}\sum_{k=1}^{3}\mu_k\omega_k(\xi_k)=0,\quad \mathrm{Re}\sum_{k=1}^{3}\delta_k\omega_k(\xi_k)=0 \quad \text{for } |\xi_k|=1 \tag{34}$$

which can be written in matrix form as,

$$\begin{Bmatrix}\bar{\omega}_1\\ \bar{\omega}_2\\ \bar{\omega}_3\end{Bmatrix}=\begin{bmatrix}E_{11} & E_{12} & E_{13}\\ E_{21} & E_{22} & E_{23}\\ E_{31} & E_{32} & E_{33}\end{bmatrix}\begin{Bmatrix}\omega_1\\ \omega_2\\ \omega_3\end{Bmatrix} \quad \text{for} \quad |\xi_k|=1 \tag{35}$$

$$\text{where } \begin{bmatrix}E_{11} & E_{12} & E_{13}\\ E_{21} & E_{22} & E_{23}\\ E_{31} & E_{32} & E_{33}\end{bmatrix}=-\begin{bmatrix}1 & 1 & 1\\ \bar{\mu}_1 & \bar{\mu}_2 & \bar{\mu}_3\\ \bar{\delta}_1 & \bar{\delta}_2 & \bar{\delta}_3\end{bmatrix}^{-1}\begin{bmatrix}1 & 1 & 1\\ \mu_1 & \mu_2 & \mu_3\\ \delta_1 & \delta_2 & \delta_3\end{bmatrix}$$

Assuming $\omega_k(\xi_k)$ in a form similar to that of Eq. (28) and Substituting it into Eq. (35) yields six constraint equations on the twelve real coefficients $a_k^{(n)}, b_k^{(n)}, a_k^{(-n)}$ and $b_k^{(-n)} (k=1,2,3)$. By expressing $a_k^{(-n)}$ and $b_k^{(-n)}$ in terms of $a_k^{(n)}$ and $b_k^{(n)}$, we get:

$$\begin{aligned} a_k^{(-n)} &= \sum_{j=1}^{3}\left[\mathrm{Re}(E_{kj})a_j^{(n)} - Im(E_{kj})b_j^{(n)}\right],\\ b_k^{(-n)} &= -\sum_{j=1}^{3}\left[Im(E_{kj})a_j^{(n)} + \mathrm{Re}(E_{kj})b_j^{(n)}\right] \end{aligned} \tag{36}$$

So the number of Trefftz functions m_T is reduced to $m_T = 6(M+1)$.

Substituting Eq. (36) into Eqs. (29)–(31) yields the following *special set* of Trefftz functions:

$$\begin{aligned} \underline{\mathbf{u}}_{void} &= \sum_{n=0}^{\infty}\sum_{k=1}^{3}\left[\Phi_{a_k}^{(n)}a_k^{(n)} + \Phi_{b_k}^{(n)}b_k^{(n)}\right],\\ \underline{\boldsymbol{\sigma}}_{void} &= \sum_{n=0}^{\infty}\sum_{k=1}^{3}\left[\Psi_{a_k}^{(n)}a_k^{(n)} + \Psi_{b_k}^{(n)}b_k^{(n)}\right]\\ \underline{\boldsymbol{\varepsilon}}_{void} &= \sum_{n=0}^{\infty}\sum_{k=1}^{3}\left[\Gamma_{a_k}^{(n)}a_k^{(n)} + \Gamma_{b_k}^{(n)}b_k^{(n)}\right] \end{aligned} \tag{37}$$

where:

$$\begin{aligned} \Phi_{a_k}^{(n)} &= \chi_{a_k}^{(n)} + \sum_{j=1}^{3}\left[\mathrm{Re}(E_{jk})\chi_{a_j}^{(-n)} - \mathrm{Im}(E_{jk})\chi_{b_j}^{(-n)}\right],\\ \Phi_{b_k}^{(n)} &= \chi_{b_k}^{(n)} - \sum_{j=1}^{3}\left[\mathrm{Im}(E_{jk})\chi_{a_j}^{(-n)} + \mathrm{Re}(E_{jk})\chi_{b_j}^{(-n)}\right]\\ \Psi_{a_k}^{(n)} &= \Sigma_{a_k}^{(n)} + \sum_{j=1}^{3}\left[\mathrm{Re}(E_{jk})\Sigma_{a_j}^{(-n)} - \mathrm{Im}(E_{jk})\Sigma_{b_j}^{(-n)}\right],\\ \Psi_{b_k}^{(n)} &= \Sigma_{b_k}^{(n)} - \sum_{j=1}^{3}\left[\mathrm{Im}(E_{jk})\Sigma_{a_j}^{(-n)} + \mathrm{Re}(E_{jk})\Sigma_{b_j}^{(-n)}\right]\\ \Gamma_{a_k}^{(n)} &= \Upsilon_{a_k}^{(n)} + \sum_{j=1}^{3}\left[\mathrm{Re}(E_{jk})\Upsilon_{a_j}^{(-n)} - \mathrm{Im}(E_{jk})\Upsilon_{b_j}^{(-n)}\right],\\ \Gamma_{b_k}^{(n)} &= \Upsilon_{b_k}^{(n)} - \sum_{j=1}^{3}\left[\mathrm{Im}(E_{jk})\Upsilon_{a_j}^{(-n)} + \mathrm{Re}(E_{jk})\Upsilon_{b_j}^{(-n)}\right] \end{aligned} \tag{38}$$

and in (38):

$$\begin{aligned} \chi_{a_k}^{(\pm n)} &= 2\mathrm{Re}(\mathcal{D}_k)\mathrm{Re}\left(\xi_k^{\pm n}\right) - 2\mathrm{Im}(\mathcal{D}_k)\mathrm{Im}\left(\xi_k^{\pm n}\right),\\ \chi_{b_k}^{(\pm n)} &= -2\mathrm{Re}(\mathcal{D}_k)\mathrm{Im}\left(\xi_k^{\pm n}\right) - 2\mathrm{Im}(\mathcal{D}_k)\mathrm{Re}\left(\xi_k^{\pm n}\right)\\ \Sigma_{a_k}^{(\pm n)} &= \pm 2n\left[\mathrm{Re}(\mathcal{G}_k)\mathrm{Re}\left(\frac{\xi_k^{\pm n-1}}{z_k'}\right) - \mathrm{Im}(\mathcal{G}_k)\mathrm{Im}\left(\frac{\xi_k^{\pm n-1}}{z_k'}\right)\right]\\ \Sigma_{b_k}^{(\pm n)} &= \mp 2n\left[\mathrm{Re}(\mathcal{G}_k)\mathrm{Im}\left(\frac{\xi_k^{\pm n-1}}{z_k'}\right) + \mathrm{Im}(\mathcal{G}_k)\mathrm{Re}\left(\frac{\xi_k^{\pm n-1}}{z_k'}\right)\right]\\ \Upsilon_{a_k}^{(\pm n)} &= \pm 2n\left[\mathrm{Re}(\mathcal{H}_k)\mathrm{Re}\left(\frac{\xi_k^{\pm n-1}}{z_k'}\right) - \mathrm{Im}(\mathcal{H}_k)\mathrm{Im}\left(\frac{\xi_k^{\pm n-1}}{z_k'}\right)\right]\\ \Upsilon_{b_k}^{(\pm n)} &= \mp 2n\left[\mathrm{Re}(\mathcal{H}_k)\mathrm{Im}\left(\frac{\xi_k^{\pm n-1}}{z_k'}\right) + \mathrm{Im}(\mathcal{H}_k)\mathrm{Re}\left(\frac{\xi_k^{\pm n-1}}{z_k'}\right)\right] \end{aligned}$$

Note that for the case of elliptical boundary, using the following ellipse parametric equation:

$$x_1(t)=a_o\cos t;\quad x_3(t)=b_o\sin t; \tag{39}$$

ds can be written in terms of the parameter t:

$$ds=\sqrt{dx_1^2+dx_3^2}=Jdt=\left(\sqrt{a_o^2\sin^2 t+b_o^2\cos^2 t}\right)dt \tag{40}$$

where J is the Jacobian of the transformation. Then any boundary integration can be written as a function of t as follows:

$$\oint_{\partial\Omega_c^e} f(\xi_k)ds=\int_{t=0}^{t=2\pi} f(\xi_k(t))Jdt \tag{41}$$

where $\xi_k(t)=\frac{z_k(t)\pm\sqrt{(z_k(t))^2-\left(a_o^2+\mu_k^2b_o^2\right)}}{a_o-i\mu_k b_o}$, $z_k(t)=x_1(t)+\mu_k x_3(t)$.

In the following, the finite element formulation of the new proposed TLG grains is presented. All the variables should be expressed in the grain's Cartesian local coordinate system ($\hat{x}_1-\hat{x}_3$ is Fig. 1 (left)), hence tensor transformation rule can be used again to do this rotation by an angle $-(\zeta+\gamma)$.

4. Formulation of Trefftz-Lekhnitskii Grains (TLGs) for piezoelectric materials with/without void

Consider a 2D irregular m-sided polygonal grain with/without a void as shown in Fig. 1 (left). We can define linear displacements and electric potential fields along each grain boundary in terms of the nodal values of the mechanical displacements $\mathbf{q}_{\mathbf{u}i}$ and electric potential $\mathbf{q}_{\boldsymbol{\varphi}}$, as:

$$\tilde{\mathbf{u}}=\tilde{\mathbf{N}}_{\mathbf{u}}\mathbf{q}_{\mathbf{u}},\tilde{\varphi}=\tilde{\mathbf{N}}_{\boldsymbol{\varphi}}\mathbf{q}_{\boldsymbol{\varphi}} \text{ or } \underline{\tilde{\mathbf{u}}}=\begin{Bmatrix}\tilde{\mathbf{u}}\\ \tilde{\varphi}\end{Bmatrix}=\begin{bmatrix}\tilde{\mathbf{N}}_{\mathbf{u}} & \mathbf{0}\\ \mathbf{0} & \tilde{\mathbf{N}}_{\boldsymbol{\varphi}}\end{bmatrix}\begin{Bmatrix}\mathbf{q}_{\mathbf{u}}\\ \mathbf{q}_{\boldsymbol{\varphi}}\end{Bmatrix}=\tilde{\mathbf{N}}\mathbf{q} \text{ at } \partial\Omega^e \tag{42}$$

where $\tilde{\mathbf{N}}_{\mathbf{u}}$ and $\tilde{\mathbf{N}}_{\boldsymbol{\varphi}}$ are shape functions, $\underline{\tilde{\mathbf{u}}}=[\tilde{u}_1 \quad \tilde{u}_3 \quad \tilde{\varphi}]^T$ and $\mathbf{q}^T=\begin{Bmatrix}\mathbf{q}_{\mathbf{u}}^T & \mathbf{q}_{\boldsymbol{\varphi}}^T\end{Bmatrix}$.

The basic solution set in Eqs. (29) and (30) can be used as the interior/exterior fields, which satisfy the constitutive law, the strain–displacement relationship, the electric field-electric potential relationship and the equilibrium and Gauss's equations. For the case of impermeable elliptical voids, the special solution set in Eq. (37) which satisfies the void stress-free charge-free boundary conditions can be used instead. In matrix and vector notation, these interior/exterior fields can be written in the form:

$$\begin{Bmatrix}\mathbf{u}\\ \varphi\end{Bmatrix}=\begin{Bmatrix}\mathbf{N}_{\mathbf{u}}\\ \mathbf{N}_{\varphi}\end{Bmatrix}\boldsymbol{\alpha},\begin{Bmatrix}\boldsymbol{\sigma}\\ \mathbf{D}\end{Bmatrix}=\begin{Bmatrix}\mathbf{M}_{\boldsymbol{\sigma}}\\ \mathbf{M}_{\mathbf{D}}\end{Bmatrix}\boldsymbol{\alpha}, \text{ in } \Omega^e \text{ or } \underline{\mathbf{u}}=\mathbf{N}\boldsymbol{\alpha}, \ \underline{\boldsymbol{\sigma}}=\mathbf{M}\boldsymbol{\alpha}, \text{ in } \Omega^e \tag{43}$$

where $\mathbf{N}$ contains Trefftz functions in the order of $M_s, \ldots, 0, 1, \ldots, M$ and $\boldsymbol{\alpha}$ denotes the unknown real coefficients ($a_k^{(\pm n)}, b_k^{(\pm n)}$, $k=1, 2, 3$ and $n=M_s, \ldots, M$) associated with Trefftz functions. If there is no void, only the non-negative exponents are used.

The tractions and density of free charge on the boundaries can be written as:

$$\mathbf{t} = \mathbf{n}_\sigma \boldsymbol{\sigma} = \mathbf{n}_\sigma \mathbf{M}_\sigma \boldsymbol{\alpha}, \quad Q = \mathbf{n}_e \mathbf{D} = \mathbf{n}_e \mathbf{M}_\mathbf{D} \boldsymbol{\alpha} \quad \text{at } \partial\Omega^e,$$
$$\text{or} \quad \underline{\mathbf{t}} = \begin{Bmatrix} \mathbf{t} \\ Q \end{Bmatrix} = \begin{bmatrix} \mathbf{n}_\sigma & \mathbf{0} \\ \mathbf{0} & \mathbf{n}_e \end{bmatrix} \begin{Bmatrix} \boldsymbol{\sigma} \\ \mathbf{D} \end{Bmatrix} = \underline{\mathbf{n}}\underline{\boldsymbol{\sigma}} = \underline{\mathbf{n}}\mathbf{M}\boldsymbol{\alpha} \quad \text{at } \partial\Omega^e, \tag{44}$$

Since the matrix interior fields already satisfy the equilibrium and Gauss's Eq. (1), the constitutive Eq. (3), as well as the strain-mechanical displacement, and electric field-electric potential relations (Eq. (2)), three steps should be done:

1. Step one: matrix interior primal fields should be related to matrix boundary primal fields. Once the mechanical displacements and the electric potential are expressed in terms of their nodal values in each grain, the displacement and the electric potential continuities (Eq. (8)) are automatically satisfied, and the essential boundary conditions (in Eqs. (5) and (6)) can be easily enforced after generating the global system of equations.
2. Step two: the reciprocity conditions (Eq. (9)) as well as the natural boundary conditions (Eqs. (5) and (6)) should be enforced.
3. Step three: (if a void exists in the grain) the conditions on the void boundary should also be satisfied as mentioned in Section 2.

There are at least three ways to accomplish step one: using multi-field boundary variational principle, using collocation method and using the least squares method. If a void exists in the grain, then we can use two methods to satisfy step three: using the special solution set as presented in subsection 3.2, or the collocation/least squares method. In the following, we present different Trefftz-Lekhnitskii Grains (TLGs) with/without voids. Table 1 presents the considered grains and the methods used to satisfy the previously mentioned conditions. When the void boundary $\partial\Omega_c^e$ shrinks to zero, the grain is reduced to the case of a piezoelectric grain with no void.

It should be noted that the three grain types that are based on the special solution set (TLG-BVPs, TLG-Cs, TLG-LSs) are expected to be more efficient than the other grain-types, because the special solution set already satisfies the void boundary conditions and there is no need to collocate along the void boundary. However, the special solution set is only valid for the case of traction-free, charge-free voids and it is not available in the literature for other cases. Actually, these grains are not valid if the void is pressurized, filled with conducting fluid or if the void is replaced by any type of inclusions. This is why it is important to consider the other grain types which will be extended to handle the aforementioned cases in a future work.

4.1. Using multi-field boundary variational principle

Using the special solution set that satisfies the void boundary conditions if the grain contains a void, or the basic solution set for interior domains if the grain contains no void, then a multi-field boundary variational principle whose Euler–Lagrange equations (stationarity conditions) are the natural BCs, the reciprocity conditions, as well as the compatibility between interior and boundary primal fields can be used to derive the grain equation.

$$\Pi_1(u_i, \tilde{u}_i, \varphi, \tilde{\varphi}) = \sum_{e=1}^{N} \left\{ -\int_{\partial\Omega^e} \frac{1}{2}(t_i u_i + Q\varphi) dS + \int_{\partial\Omega^e} (t_i \tilde{u}_i + Q\tilde{\varphi}) dS - \int_{S_t^e} \bar{t}_i \tilde{u}_i dS - \int_{S_Q^e} \bar{Q}\tilde{\varphi} dS \right\} \tag{45}$$

where $i = 1,3$ in Eq. (45) and the equations to follow. Euler–Lagrange equations of this functional are:

$$\begin{aligned} &t_i = n_{\sigma j}\sigma_{ij} = \bar{t}_i \text{ at } S_t^e, \quad Q = n_{ei} D_i = \bar{Q} \text{ at } S_Q^e, \\ &(n_{\sigma j}\sigma_{ij})^+ + (n_{\sigma j}\sigma_{ij})^- = 0, \quad (n_{ei}D_i)^+ + (n_{ei}D_i)^- = 0 \text{ at } S_g^e \\ &u_i^+ = u_i^- = \tilde{u}_i, \quad \varphi^+ = \varphi^- = \tilde{\varphi} \text{ at } S_g^e \end{aligned} \tag{46}$$

thus achieving the three steps simultaneously. In matrix and vector notation Π_1 can be written as:

$$\Pi_1(\underline{\mathbf{u}}, \underline{\tilde{\mathbf{u}}}) = \sum_{e=1}^{N} \left\{ -\int_{\partial\Omega^e} \frac{1}{2}\underline{\mathbf{t}} \cdot \underline{\mathbf{u}} dS + \int_{\partial\Omega^e} \underline{\mathbf{t}} \cdot \underline{\tilde{\mathbf{u}}} dS - \int_{S_t^e} \bar{\mathbf{t}} \cdot \tilde{\mathbf{u}} dS - \int_{S_Q^e} \bar{Q}\tilde{\varphi} dS \right\} \tag{47}$$

$$\Pi_1(\boldsymbol{\alpha}, \mathbf{q}) = \sum_{e=1}^{N} \begin{Bmatrix} -\boldsymbol{\alpha}^T \left(\frac{1}{2} \int_{\partial\Omega^e} \mathbf{M}^T \underline{\mathbf{n}}^T \mathbf{N} dS \right) \boldsymbol{\alpha} + \boldsymbol{\alpha}^T \left(\int_{\partial\Omega^e} \mathbf{M}^T \underline{\mathbf{n}}^T \tilde{\mathbf{N}} dS \right) \mathbf{q} \\ -\left(\int_{S_t^e} \bar{\mathbf{t}}^T \tilde{\mathbf{N}}_\mathbf{u} dS \right) \mathbf{q}_\mathbf{u} - \left(\int_{S_Q^e} \bar{Q} \tilde{\mathbf{N}}_\varphi dS \right) \mathbf{q}_\varphi \end{Bmatrix} \tag{48}$$

The variation of Π_1 is:

$$\begin{aligned} \delta\Pi_1(\delta\boldsymbol{\alpha}, \delta\mathbf{q}) &= \delta \sum_{e=1}^{N} \left\{ -\frac{1}{2}\boldsymbol{\alpha}^T \mathbf{H}_{\mathbf{mm}} \boldsymbol{\alpha} + \boldsymbol{\alpha}^T \mathbf{G}_{\mathbf{mq}} \mathbf{q} - \mathbf{q}^T \mathbf{Q} \right\} \\ &= \sum_{e=1}^{N} \left\{ -\delta\boldsymbol{\alpha}^T \mathbf{H}_{\mathbf{mm}} \boldsymbol{\alpha} + \delta\boldsymbol{\alpha}^T \mathbf{G}_{\mathbf{mq}} \mathbf{q} + \delta\mathbf{q}^T \mathbf{G}_{\mathbf{mq}}^T \boldsymbol{\alpha} - \delta\mathbf{q}^T \mathbf{Q} \right\} \\ &= \sum_{e=1}^{N} \left\{ \delta\mathbf{q}^T \left(\mathbf{G}_{\mathbf{mq}}^T \boldsymbol{\alpha} - \mathbf{Q} \right) + \delta\boldsymbol{\alpha}^T \left(\mathbf{G}_{\mathbf{mq}} \mathbf{q} - \mathbf{H}_{\mathbf{mm}} \boldsymbol{\alpha} \right) \right\} \end{aligned} \tag{49}$$

where

$$\mathbf{H}_{\mathbf{mm}} = \int_{\partial\Omega^e} \mathbf{M}^T \underline{\mathbf{n}}^T \mathbf{N} dS, \quad \mathbf{G}_{\mathbf{mq}} = \int_{\partial\Omega^e} \mathbf{M}^T \underline{\mathbf{n}}^T \tilde{\mathbf{N}} dS,$$
$$\mathbf{Q}^T = \begin{bmatrix} \int_{S_t^e} \bar{\mathbf{t}}^T \tilde{\mathbf{N}}_\mathbf{u} dS & \int_{S_Q^e} \bar{Q} \tilde{\mathbf{N}}_\varphi dS \end{bmatrix} \tag{50}$$

where the matrix interior fields to be used are those presented in Eq. (37) for the case of a grain with a void, or Eqs. (29) and (30) for interior domains for a grain with no void.

Using $\delta\Pi_1 = 0$ and for arbitrary $\delta\mathbf{q}$ and $\delta\boldsymbol{\alpha}$ we get for each grain:

$$\mathbf{G}_{\mathbf{mq}}^T \boldsymbol{\alpha} - \mathbf{Q} = \mathbf{0}, \quad \mathbf{G}_{\mathbf{mq}} \mathbf{q} - \mathbf{H}_{\mathbf{mm}} \boldsymbol{\alpha} = \mathbf{0}$$

Using the second equation to write $\boldsymbol{\alpha}$ in terms of $\mathbf{q}$ as:

$$\boldsymbol{\alpha} = \mathbf{H}_{\mathbf{mm}}^{-1} \mathbf{G}_{\mathbf{mq}} \mathbf{q} \tag{51}$$

Substituting this into the first equation to get the grain equation in terms of $\mathbf{q}$:

$$\mathbf{K}_{\mathbf{bvp}} \mathbf{q} = \mathbf{Q}, \quad \mathbf{K}_{\mathbf{bvp}} = \mathbf{G}_{\mathbf{mq}}^T \mathbf{H}_{\mathbf{mm}}^{-1} \mathbf{G}_{\mathbf{mq}} \tag{52}$$

Table 1
Different TLGs and the corresponding methods used to satisfy the different conditions (BVP refers to "Boundary variational principle" and PVP refers to "Primitive variational principle").

Grain	Matrix interior and boundary primal fields continuity	Void boundary conditions	Reciprocity and natural BCs
TLG-BVPs	BVP	Special solution set	BVP
TLG-C	Collocation	Collocation/least squares	PVP
TLG-Cs	Collocation	Special solution set	PVP
TLG-LS	Least squares	Collocation/least squares	PVP
TLG-LSs	Least squares	Special solution set	PVP

We denote this grain as "TLG-BVPs" (boundary variational principle with special solution set) for grains with voids and as "TLG-BVP" for grains with no voids. This formulation clearly involves Lagrangian multipliers and hence suffers from LBB conditions [30,31], which are impossible to be satisfied a priori. This means that the eigen vaules of the stiffness matrix of an arbitrarily distorted grain, without a void for instance, may include more than four zeros (for the three rigid-body and one constant electric potential modes) which indicates that the numerical formulation of the grain is not always stable. The stiffness matrix of TLG-BVPs (or TLG-BVP) grain requires integration along the grain boundary to evaluate $\mathbf{G_{mq}}$ and $\mathbf{H_{mm}}$, as well as matrix inversion ($\mathbf{H_{mm}}$).

Note that the first six Trefftz functions (corresponding to $n = 0$) should be eliminated from $\mathbf{N}$ and $\mathbf{M}$ when using this method because they correspond to rigid-body modes which do not contribute to the strain energy stored in the grain.

4.2. Using collocation method

In this method, the continuity between the matrix interior and boundary primal fields (electromechanical displacements) are enforced in a strong sense at several pre-selected collocation points $\mathbf{x}^{(r)}$, $r = 1, 2, \ldots, R$ along the grain boundary $\partial\Omega^e$ (this is in contrast to the boundary variational principle where this compatibility was enforced in a variational sense through the use of Lagrangian multipliers which renders the formulation plagued by LBB conditions). Also when using the basic solution set (Eqs. (29)–(31)), the void boundary conditions are enforced by dividing the void periphery into number of curved segments, n_s, along the void boundary $\partial\Omega_c^e = \sum_{j=1}^{n_s} \partial\Omega_{cj}^e$, and enforcing the boundary conditions on each segment. So,

(1) Compatibility between matrix interior and boundary primal fields along $\partial\Omega^e$:

$$\underline{\mathbf{u}}(\mathbf{x}^{(r)}, \boldsymbol{\alpha}) = \underline{\tilde{u}}(\mathbf{x}^{(r)}, \mathbf{q}), \quad \mathbf{x}^{(r)} \in \partial\Omega^e \quad r = 1, 2, \ldots, R \tag{53}$$

(2) Traction-free and charge-free conditions along $\partial\Omega_c^e$:

$$\int_{\partial\Omega_{cj}^e} \mathbf{t}(\mathbf{x}, \boldsymbol{\alpha}) ds = 0, \quad j = 1, 2, \ldots, n_s \tag{54}$$

By selecting enough number of void boundary segments, and solving (53) and (54) in a least-square sense, $\boldsymbol{\alpha}$ is related to $\mathbf{q}$ as follows:

$$\mathbf{A}\boldsymbol{\alpha} = \mathbf{B}\mathbf{q} \quad \text{or} \quad \boldsymbol{\alpha} = \mathbf{A}^{-1}\mathbf{B}\mathbf{q} = \mathbf{Z}\mathbf{q} \tag{55}$$

Now, the interior fields are related to nodal primal variables (step one), and the void boundary conditions are enforced (step three), we just need to enforce the natural boundary conditions as well as the reciprocity conditions on the outer boundary (step two) using the following simple primitive field variational principle:

$$\Pi_2(u_i, \varphi) = \sum_{e=1}^{N} \left\{ \int_{\partial\Omega^e} \frac{1}{2}(t_i u_i + Q\varphi) dS - \int_{S_t^e} \bar{t}_i u_i dS - \int_{S_Q^e} \overline{Q}\varphi dS \right\} \tag{56}$$

Whose Euler–Lagrange equations are:

$$\begin{aligned} &t_i = n_{\sigma j}\sigma_{ij} = \bar{t}_i \text{ at } S_t^e, \quad Q = n_{ei}D_i = \overline{Q} \text{ at } S_Q^e, \\ &(n_{\sigma j}\sigma_{ij})^+ + (n_{\sigma j}\sigma_{ij})^- = 0, \quad (n_{ei}D_i)^+ + (n_{ei}D_i)^- = 0 \text{ at } S_g^e \end{aligned} \tag{57}$$

In matrix and vector notation Π_2 can be written as:

$$\Pi_2(\underline{\mathbf{u}}) = \sum_{e=1}^{N} \left\{ \int_{\partial\Omega^e} \frac{1}{2}\mathbf{t}\cdot\underline{\mathbf{u}} dS - \int_{S_t^e} \bar{\mathbf{t}}\cdot\mathbf{u} dS - \int_{S_Q^e} \overline{Q}\varphi dS \right\} \tag{58}$$

$$\begin{aligned} \Pi_2(\mathbf{q}) &= \sum_{e=1}^{N} \left\{ \frac{1}{2}\mathbf{q}^T\mathbf{Z}^T \left(\int_{\partial\Omega^e} \mathbf{M}^T\underline{\mathbf{n}}^T\mathbf{N} dS \right)\mathbf{Z}\mathbf{q} - \left[\int_{S_t^e} \bar{\mathbf{t}}^T\tilde{\mathbf{N}}_{\mathbf{u}} dS \;\; \int_{S_Q^e} \overline{Q}\tilde{\mathbf{N}}_{\varphi} dS \right]\mathbf{q} \right\} \\ &= \sum_{e=1}^{N} \left\{ \frac{1}{2}\mathbf{q}^T\mathbf{Z}^T\mathbf{H}_{\mathbf{mm}}\mathbf{Z}\mathbf{q} - \mathbf{q}^T\mathbf{Q} \right\} \end{aligned} \tag{59}$$

The variation of Π_2 is:

$$\begin{aligned} \delta\Pi_2(\delta\mathbf{q}) &= \sum_{e=1}^{N} \left\{ \delta\mathbf{q}^T(\mathbf{Z}^T\mathbf{H}_{\mathbf{mm}}\mathbf{Z})\mathbf{q} - \delta\mathbf{q}^T\mathbf{Q} \right\} \\ &= \sum_{e=1}^{N} \left\{ \delta\mathbf{q}^T\mathbf{K}_{\mathbf{c}}\mathbf{q} - \delta\mathbf{q}^T\mathbf{Q} \right\} \end{aligned} \tag{60}$$

where $\mathbf{K_c} = \mathbf{Z}^T\mathbf{H_{mm}}\mathbf{Z}$ is the stiffness matrix of "TLG-C" grain. This grain does not suffer from LBB conditions, because there is no Lagrangian multipliers involved. In order to obtain the stiffness matrix of this grain, only one matrix, $\mathbf{H_{mm}}$, requires integration over the outer boundary, as well as the evaluation of $\mathbf{Z}$.

For an impermeable elliptical void, the special solution set (Eq. (37)) can be used as an alternative to the collocation method to enforce the traction-free, charge-free conditions on the void periphery. In this case, Eq. (54) is not used in obtaining $\boldsymbol{\alpha}$ in Eq. (55). This grain is denoted as "TLG-Cs".

4.3. Using the least squares method

When the number of collocation points is increased to a limit of infinity, it is equivalent to enforcing the compatibility between boundary and interior primal fields using the least squares method; that is minimizing the functional $L_1(\underline{\mathbf{u}}, \underline{\tilde{\mathbf{u}}})$:

$$\begin{aligned} L_1(\underline{\mathbf{u}}, \underline{\tilde{\mathbf{u}}}) &= \int_{\partial\Omega^e} (\underline{\mathbf{u}} - \underline{\tilde{\mathbf{u}}})^T(\underline{\mathbf{u}} - \underline{\tilde{\mathbf{u}}}) dS \\ L_1(\boldsymbol{\alpha}, \mathbf{q}) &= \int_{\partial\Omega^e} \left(\boldsymbol{\alpha}^T\mathbf{N}^T\mathbf{N}\boldsymbol{\alpha} - 2\boldsymbol{\alpha}^T\mathbf{N}^T\tilde{\mathbf{N}}\mathbf{q} + \mathbf{q}^T\tilde{\mathbf{N}}^T\tilde{\mathbf{N}}\mathbf{q} \right) dS \\ &= \boldsymbol{\alpha}^T\mathbf{A_1}\boldsymbol{\alpha} - 2\boldsymbol{\alpha}^T\mathbf{B_1}\mathbf{q} + \mathbf{q}^T\mathbf{D_1}\mathbf{q} \end{aligned} \tag{61}$$

where $\mathbf{A_1} = \int_{\partial\Omega^e} \mathbf{N}^T\mathbf{N} dS$, $\mathbf{B_1} = \int_{\partial\Omega^e} \mathbf{N}^T\tilde{\mathbf{N}} dS$ and $\mathbf{D_1} = \int_{\partial\Omega^e} \tilde{\mathbf{N}}^T\tilde{\mathbf{N}} dS$.

To minimize $L_1(\boldsymbol{\alpha}, \mathbf{q})$ for a fixed $\mathbf{q}$, we have:

$$\delta L_1(\delta\boldsymbol{\alpha}, \mathbf{q}) = 2\delta\boldsymbol{\alpha}^T\mathbf{A_1}\boldsymbol{\alpha} - 2\delta\boldsymbol{\alpha}^T\mathbf{B_1}\mathbf{q} = 0 \tag{62}$$

This should be true for any $\delta\boldsymbol{\alpha}$, hence together with Eq. (54) that enforces the void BCs, we obtain $\boldsymbol{\alpha}$:

$$\begin{bmatrix} \mathbf{A_1} \\ \mathbf{A_2} \end{bmatrix}\boldsymbol{\alpha} = \begin{bmatrix} \mathbf{B_1} \\ \mathbf{0} \end{bmatrix}\mathbf{q} \quad \text{or} \quad \boldsymbol{\alpha} = \mathbf{Z_1}\mathbf{q} \tag{63}$$

Eq. (63) is to be used instead of Eq. (55), and hence all the steps used in constructing TLG-C grain are exactly the same by replacing $\mathbf{Z}$ by $\mathbf{Z_1}$ in all equations following Eq. (55) in the previous subsection where the functional $\Pi_2(\mathbf{q})$ was used to derive the grain equation. This grain is labeled as "TLG-LS". Note that this method requires additional integration in evaluating $\mathbf{A_1}$and $\mathbf{B_1}$ as well as matrix inversion. Again, when using the special solution set (Eq. (37)) to enforce the void boundary conditions instead of collocating at the void boundary, the resulting grain is denoted as "TLG-LSs".

4.4. On the selection of the maximum order of Trefftz functions

There are two conditions that should be considered in determining the maximum order of Trefftz functions, M, to be used in developing TLG grains. These two conditions are:

1. The number of Trefftz functions (or undetermined coefficients) m_T should be larger than the number of the grain's degrees of freedom (DOF) in order to ensure that the number of independent Trefftz modes are larger than or equal to the number of the grain's DOFs. Note that Trefftz formulation (Eqs. (29) and (30) or

Eq. (37)) generates some repeated modes. For example, and as mentioned earlier, the first 6 Trefftz functions (corresponding to $n = 0$) corresponds to 4 rigid-body modes (two translational, one rotational and one constant electric potential mode). The number of degrees of freedom in any grain equals to the number of nodes $\times$ the number of degrees of freedom per node i.e. $3m$. Hence for rank sufficiency of the grain, the number of non-rigid-body Trefftz modes, $6M$ (or $12M$ when using the basic solution set for exterior domains), should be larger than the number of non-rigid-body degrees of freedom which is $3m - 4$. This ensures that all grain types except TLG-BVP (or TLG-BVPs) are stable or rank sufficient (it is impossible to ensure this for TLG-BVP grain because the grain formulation involves Lagrangian multipliers as mentioned earlier).

2. The number of equations used to solve for the undetermined coefficients should be larger than or equal to the number of these undetermined coefficients (m_T). In developing TLG-C (for grains with no voids) and TLG-Cs, we should select the number of collocation points used with any m-sided grain. Each collocation point provides 3 equations since we are collocating the 3 primal variables (the 2 mechanical displacements and the electric potential). If we use only 2 collocation points per edge then the total number of collocation equations in any m-sided polygonal grain is $m \times 2 \times 3 = 6m$. For TLG-C grains with voids where the basic solution set is to be used, $m_T = 6(2M + 1)$ because the negative exponents are also considered, thus increasing the number of unknowns; however $3n_s$ additional equations are added to enforce the void boundary conditions on the void periphery. Here, we take $n_s = 48$ (where again n_s is the number of void boundary segments).

When using the basic solution set (interior domains) or the special solution set, these two conditions can be expressed as:

$6M > 3m - 4$ and $m_T = 6(M + 1) \leqslant 2 \times 3m$

When using the basic solution set (exterior domains), the two conditions are:

$12M > 3m - 4$ and $m_T = 6(2M + 1) \leqslant 2 \times 3m + 3n_s$

So the conditions on the maximum order of Trefftz functions can be written as:

$$\begin{aligned} &\frac{3m-4}{6} < M \leq m-1 \text{ when using basic solution set (interior domains) or special solution set} \\ &\frac{3m-4}{12} < M \leq \frac{2m+n_s-2}{4} \text{ when using basic solution set (exterior domains)} \end{aligned} \tag{64}$$

When using the basic solution set (interior domains) or the special solution set, we can use $M = \left\lceil \frac{3m-4}{6} \right\rceil$, where $\lceil\,\rceil$ is a function that rounds a number up to an integer. This satisfies the two conditions. In this work we also use $M = \left\lceil \frac{3m+2}{6} \right\rceil$ which is larger by one order. This is suitable for grains with no void, or for grains with void and based on the special solution set. When using the basic solution set (exterior domains), larger values of M are to be used to increase the accuracy of the solution without violating the second condition.

Eq. (55) in TLG-C and TLG-Cs grains is over-constrained whenever the number of collocation points exceeds the number of undetermined coefficients, m_T. In addition, the system of matrices in both TLG-C and TLG-LS (Eqs. (55) and (63)) are singular because of the repeated Trefftz functions. Hence in order to solve such systems, singular value decomposition (SVD) technique should be used. The SVD method can solve even the singular system of equations and produces the least squares solutions to the over-constrained systems.

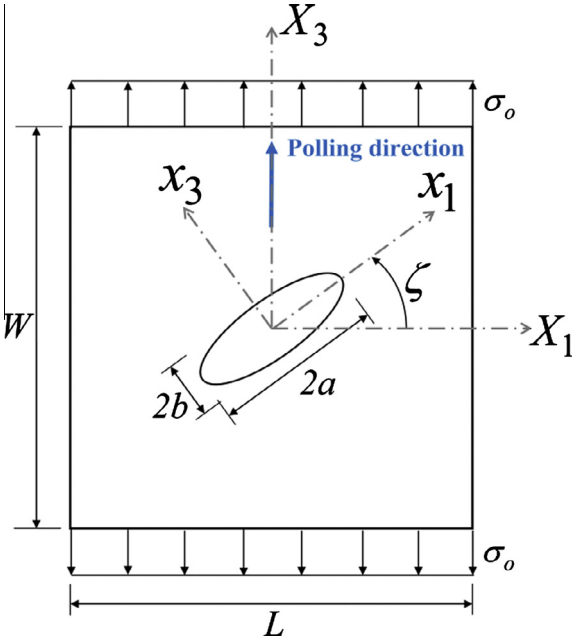

Fig. 2. A Finite rectangular domain with arbitrarily oriented elliptical void.

4.5. Conditioning of system matrices

Using the material matrices presented in Section 2 directly in any grain formulation will result in an ill-conditioned system of equations to be solved. This is because the numerical values of the components of the material stiffness matrix **C** are as large as 10^{10}, while that of the dielectric material matrix **h** are as small as 10^{-9}. Hence the ratio is as large as 10^{19}, and this makes the global stiffness matrix of the grain ill-conditioned. To improve the conditioning we can use the following conditioned constitutive equation instead of that of Eqs. (3), (11) and (12), or (13):

$$\begin{Bmatrix} \hat{\boldsymbol{\sigma}}' \\ \hat{\mathbf{D}}' \end{Bmatrix} = \begin{bmatrix} \widehat{\mathbf{C}}' & -\hat{\mathbf{e}}'^T \\ \hat{\mathbf{e}}' & \hat{\mathbf{h}}' \end{bmatrix} \begin{Bmatrix} \boldsymbol{\varepsilon}' \\ \hat{\mathbf{E}}' \end{Bmatrix} \quad \text{or} \quad \begin{Bmatrix} \boldsymbol{\varepsilon}' \\ \hat{\mathbf{E}}' \end{Bmatrix} = \begin{bmatrix} \widehat{\mathbf{S}}' & \hat{\mathbf{g}}'^T \\ -\hat{\mathbf{g}}' & \hat{\boldsymbol{\beta}}' \end{bmatrix} \begin{Bmatrix} \hat{\boldsymbol{\sigma}}' \\ \hat{\mathbf{D}}' \end{Bmatrix} \tag{65}$$

where $\hat{\sigma}'_i = \frac{\sigma'_i}{\tilde{c}}$, $\hat{D}'_i = \frac{D'_i}{\tilde{e}}$, $\hat{E}'_i = \frac{E'_i \tilde{e}}{\tilde{c}}$ and,

$$\widehat{C}'_{ij} = \frac{C'_{ij}}{\tilde{c}}, \quad \hat{e}'_{ij} = \frac{e'_{ij}}{\tilde{e}}, \quad \hat{h}'_{ij} = \frac{h'_{ij}\tilde{c}}{\tilde{e}^2}, \quad \widehat{S}'_{ij} = S'_{ij}\tilde{c}, \quad \hat{g}_{ij} = g'_{ij}\tilde{e}, \quad \hat{\beta}'_{ij} = \frac{\beta'_{ij}\tilde{e}^2}{\tilde{c}}$$

And from Eq. (2), we also have $\hat{\varphi} = \frac{\varphi \tilde{e}}{\tilde{c}}$. Here we can select $\tilde{c} = C_{11}$, and $\tilde{e} = e_{33}$.

However, even if this conditioning is done, the system of equations to be solved using any of the previous methods will still be

Table 2
Material properties used in the numerical examples.

	C'_{ij} (10^{10} N m^{-2})				e'_{ij} (C m^{-2})			h'_{ij} (10^{-9}C (V m)$^{-2}$)	
	C'_{11}	C'_{13}	C'_{33}	C'_{44}	e'_{31}	e'_{33}	e'_{15}	h'_{11}	h'_{33}
PZT-4(1)	13.9	7.43	11.3	2.56	−6.98	13.84	13.44	6	5.47
PZT-4(2)	12.6	7.43	11.5	2.56	−5.2	15.1	12.7	6.464	5.622

ill-conditioned because of the exponential growth of the term Z_k^n as n is increased, hence we introduce a characteristic length to scale the Trefftz solution set.

For an arbitrary polygonal grain as shown in Fig. 1 (left), where the coordinates of the nodes are $\left(x_1^j, x_3^j\right)$, $j = 1, 2, \ldots, N$, the center point of the polygon has coordinates (x_1^c, x_3^c). Relative to the local coordinates at the center point, we have $\hat{z}_k = \hat{x}_1 + \mu_k \hat{x}_3 = (x_1 - x_1^c) + \mu_k (x_3 - x_3^c)$, k = 1, 2, 3 and correspondingly, $\hat{\xi}_k = \frac{\hat{z}_k \pm \sqrt{\hat{z}_k^2 - \left(a_o^2 + \mu_k^2 b_o^2\right)}}{a_o - i\mu_k b_o}$. Now, Z_k^n ($\hat{z}_k$ for interior domains or $\hat{\xi}_k$ for exterior domains) will be replaced by $\left(\widehat{Z}_k / R_c\right)^n$ where:

$$R_c = \max(R_{ck}), R_{ck} = \max_j \sqrt{\left[\mathrm{Re}\left(\widehat{Z}_k^j\right)\right]^2 + \left[\mathrm{Im}\left(\widehat{Z}_k^j\right)\right]^2}, \quad j = 1, 2, \ldots, N \tag{66}$$

This is done only for terms with positive exponents. In this way, the exponential growth of Z_k^n is prevented as n is increased because $0 < \left|\widehat{Z}_k^n\right| < 1$ for any point within the grain or along the grain boundaries.

Note also that using $\widehat{Z}_k / R_c$ instead of Z_k in Eq. (24) or (29), generates $\widehat{u}_i = \frac{u_i}{R_c}$ and $\widehat{\varphi} = \frac{\varphi}{R_c} = \frac{\varphi \bar{e}}{R_c \bar{c}}$ (not u_i and $\hat{\varphi}$), so that Eq. (2) are consistent. Hence, $\{u_1 \quad u_3 \quad \hat{\varphi}\}^T = R_c \left\{\widehat{u}_1 \quad \widehat{u}_3 \quad \widehat{\varphi}\right\}^T$ should be used in Eq. (43) for terms with positive exponents.

5. Numerical examples

All grain types described above are programmed using MATLAB in a 64-bit WINDOWS operating system, and executed on a PC computer equipped with Intel Q8300 2.5 GHz CPU, and 8 GB RAM. A commercially available piezoelectric material (PZT-4) is used in this section. The material properties are listed in Table 2 from two references: Xu and Rajapakse [7] and Wang et al.[32] and denoted PZT-4(1) and PZT-4(2) respectively.

Eigen value analysis of a single grain proved that all the proposed grain types are invariant to global coordinate system rota-

Table 3
Discrete extreme error for the considered grains in different cases.

Loading	Void shape	TLG-BVPs	TLG-Cs	TLG-LSs	TLG-C	TLG-LS
Mechanical load	Circular	1.11 (10^{-3})	1.60 (10^{-3})	1.88 (10^{-3})	3.08 (10^{-3})	3.26 (10^{-3})
	Elliptic ($\zeta = 0$)	8.90 (10^{-4})	1.02 (10^{-3})	1.04 (10^{-3})	9.17 (10^{-3})	9.34 (10^{-3})
	Elliptic ($\zeta = \pi/4$)	9.12 (10^{-4})	1.09 (10^{-3})	1.34 (10^{-3})	7.14 (10^{-3})	7.48 (10^{-3})
Electrical load	Circular	1.53 (10^{-2})	3.19 (10^{-2})	3.00 (10^{-2})	6.26 (10^{-2})	8.15 (10^{-2})
	Elliptic ($\zeta = 0$)	5.50 (10^{-3})	2.95 (10^{-2})	2.85 (10^{-2})	5.37 (10^{-2})	6.22 (10^{-2})
	Elliptic ($\zeta = \pi/4$)	6.31 (10^{-3})	2.04 (10^{-2})	1.75 (10^{-2})	2.12 (10^{-2})	2.91 (10^{-2})
Average time (sec.)		0.0584	0.0695	0.0602	0.172	0.165

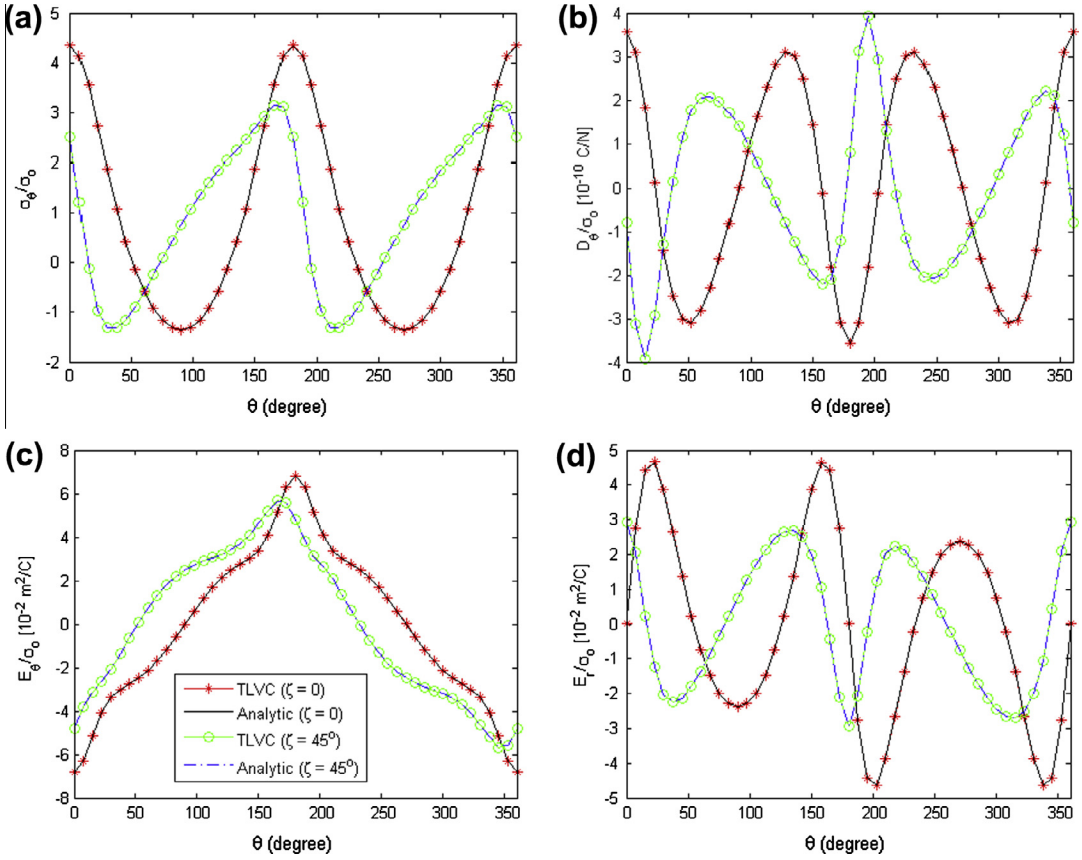

Fig. 3. Variations of (a) σ_θ/σ_o, (b) D_θ/σ_o, (c) E_θ/σ_o, (d) E_r/σ_o along the periphery of the elliptical void with $\zeta = 0$ and $\zeta = \pi/4$ in an infinite piezoelectric medium under mechanical loading.

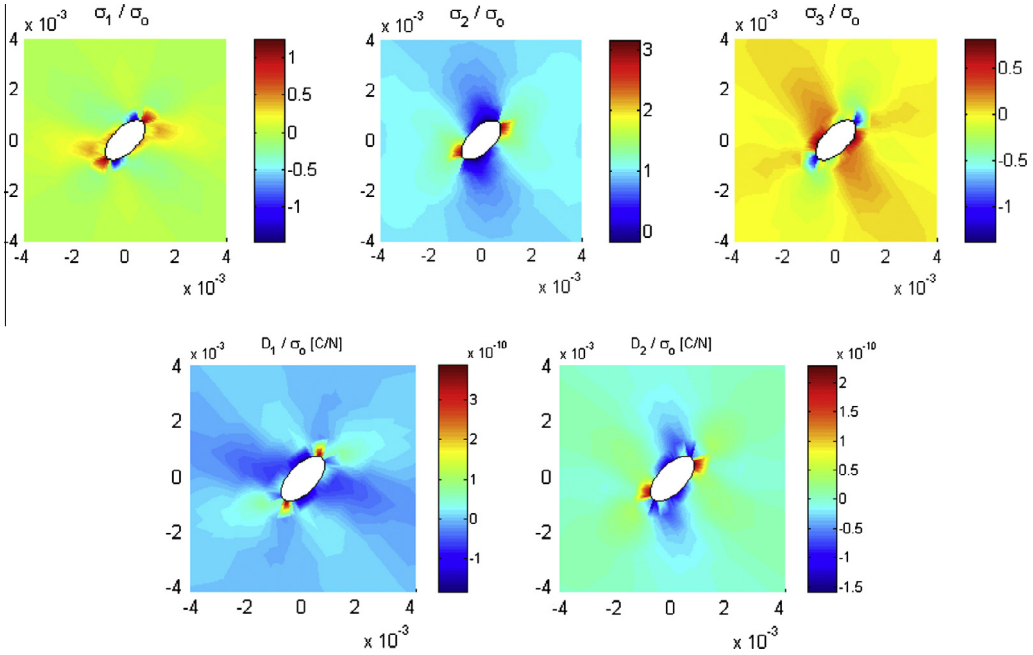

Fig. 4. Distribution of the components of stress and electric displacement around the elliptical void with $\zeta = \pi/4$ in an infinite piezoelectric medium under mechanical loading.

tion (whatever the rotation, we get exactly the same eigenvalues). Regarding stability, it is guaranteed that TLG-C, TLG-Cs, TLG-LS and TLG-LSs are stable (or rank sufficient) for any grain shape, because these types of grains avoid LBB conditions completely. However, it is not guaranteed that TLG-BVP grain is stable (has only 4 zero eigenvalues equivalent to the four rigid-body modes) for any other

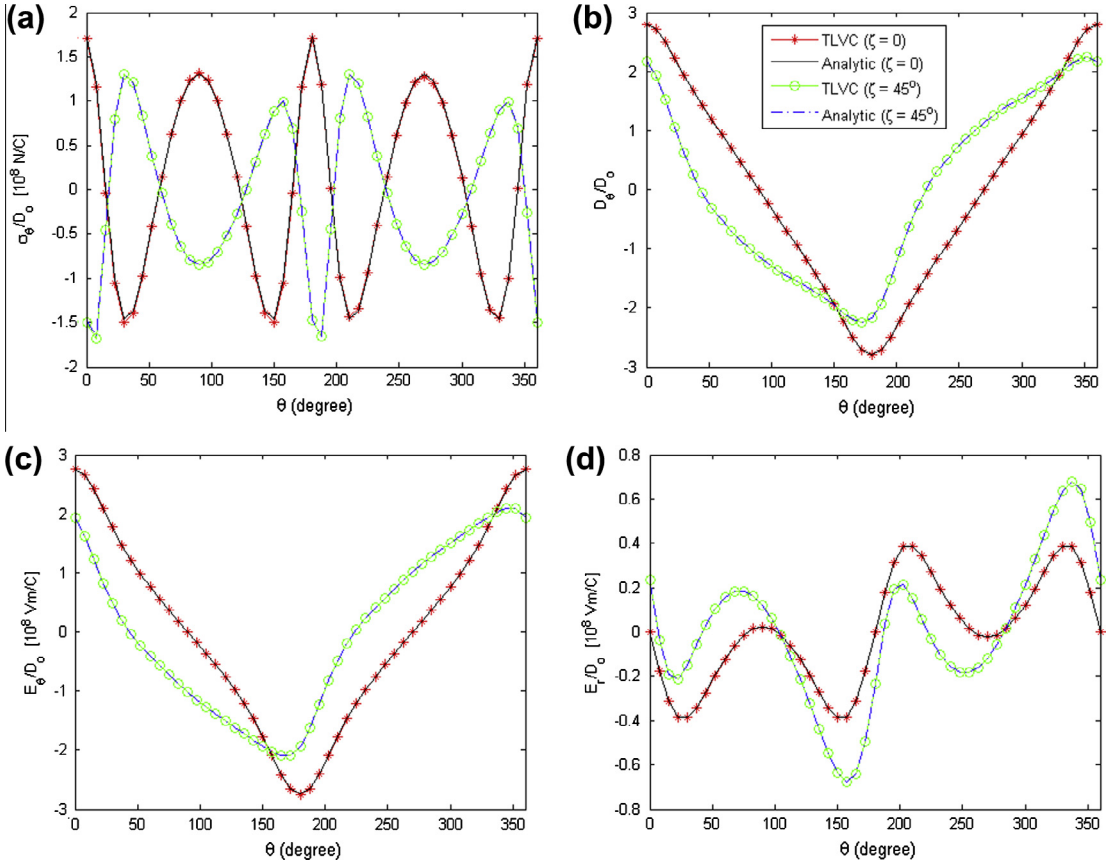

Fig. 5. Variations of (a) σ_θ/D_o, (b) D_θ/D_o, (c) E_θ/D_o, (d) E_r/D_o along the periphery of the elliptical void with $\zeta = 0$ and $\zeta = \pi/4$ in an infinite piezoelectric medium under electrical loading.

arbitrarily shaped grain, because this type of grain is plagued by LBB conditions of stability. Simple problems that use grains with no voids, such as patch test and bending of a meso-scale piezoelectric panel, can be easily and accurately modeled using any grain type and any number of grains (with no voids) to mesh the problem domain, and the error in the whole structure is less than 1%.

In the following, we show some numerical examples using the proposed TLG grains. First we present a piezoelectric domain with an impermeable horizontal or inclined elliptical void under mechanical or electrical loadings, followed by evaluation of the material properties of porous piezoelectric material as functions of porosity volume fraction. Finally we present contour plots that detect damage-prone sites in a porous piezoelectric material.

5.1. Infinite piezoelectric domain with impermeable arbitrarily-oriented elliptical void under mechanical or electrical loading

Consider an infinite piezoelectric plane with an arbitrarily oriented elliptical void subjected to vertical mechanical or electrical loading in the far field. For numerical implementations, the infinite

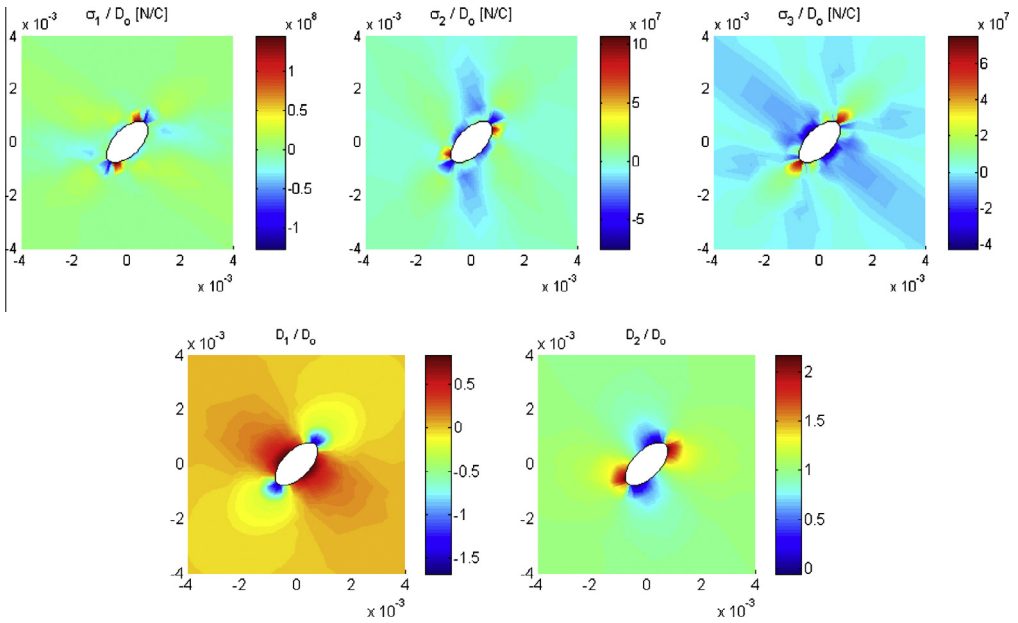

Fig. 6. Distribution of the components of stress and electric displacement around the elliptical void with $\zeta = \pi/4$ in an infinite piezoelectric medium under electrical loading.

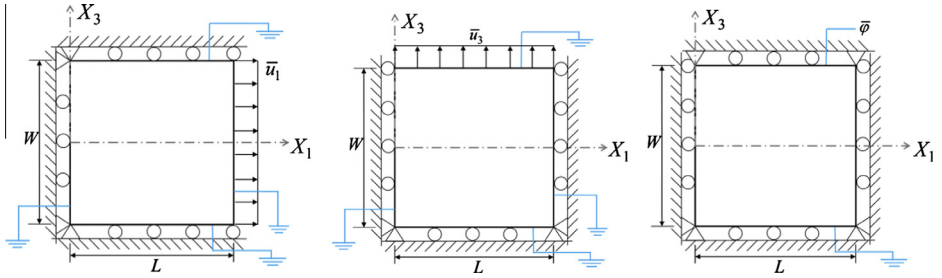

Fig. 7. Computational models used to evaluate the effective properties: (left) C_{11}^{eff} and C_{13}^{eff}, (middle) C_{33}^{eff} and C_{13}^{eff}, (right) e_{31}^{eff}, e_{33}^{eff} and h_{33}^{eff}.

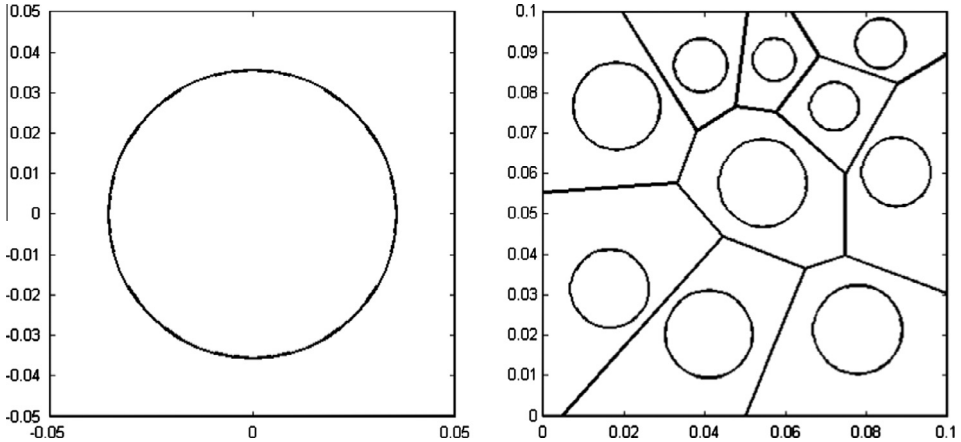

Fig. 8. Two representative volume elements (RVEs) used in the simulations.

domain is truncated into a rectangle with length L and width W, as shown in Fig. 2. The semi-axes of the elliptical void are a and b and the inclination angle between the elliptical void minor axis and the polling direction is ζ. The local coordinate system of the ellipse is denoted $x_1 - x_3$, while the global coordinate system is denoted $X_1 - X_3$. The polling direction is aligned with the global vertical X_3 axis (shown in blue in the figure). The material is PZT-4(1) whose properties are presented in Table 2 and plane strain assumption is used in this problem. Here we take $L = W = 50a$, $\sigma_o = 1$ Pa for the mechanical loading problem and $Q = 1$ C/m^2 for the electrical problem.

Table 3 shows the discrete extreme error defined in Eq. (67) for the five considered grain types where we used $M = 2$ for TLG-BVPs, TLG-Cs and TLG-LSs and $M = 5$ for the other two types. The table presents the results for both mechanical and electrical loadings and for the cases of circular hole and elliptical hole with $b/a = 2$ and $\zeta = 0$, $\pi/4$. The last row in the table also shows the average computational time in calculating the stiffness matrices of the proposed grains.

$$E^e = \max_{\mathbf{x}_i \in \partial\Omega_c} \left(\frac{\left|\sigma_\theta(\mathbf{x}_i) - \tilde{\sigma}_\theta(\mathbf{x}_i)\right|}{\tilde{\sigma}_{\max}}, \quad \frac{\left|D_\theta(\mathbf{x}_i) - \widetilde{D}_\theta(\mathbf{x}_i)\right|}{\widetilde{D}_{\max}} \right) \tag{67}$$

where $\tilde{\sigma}_\theta(\mathbf{x}_i)$ and $\widetilde{D}_\theta(\mathbf{x}_i)$ are the exact solutions at boundary points $\mathbf{x}_i$ along the periphery of the void; $\tilde{\sigma}_{\max}$ and $\widetilde{D}_{\max}$ are respectively the maximum magnitudes of $\tilde{\sigma}_\theta(\mathbf{x}_i)$ and $\widetilde{D}_\theta(\mathbf{x}_i)$.

It can be seen from the table that TLG-C and TLG-LS are more expensive than the other three grain types when $M = 5$ is used with the basic solution set. However, and as mentioned before, the formulation of only these two grain types can be extended to other void/inclusion boundary condition cases.

Figs. 3 and 5 show the computed circumferential distributions of σ_θ, D_θ, E_θ and E_r divided by σ_o (for mechanical loading) or D_o (for electrical loading) for $\zeta = 0$ and $\zeta = \pi/4$ using one TLG grain of any type (all types give very similar results). The analytical solution [7] is also included for comparison.

Perfect agreement with the analytical solution can be seen from the table and the figures. The effects of varying ζ, a/b and W/a ratios on the stress, electric displacement and electric field are presented in [22].

Figs. 4 and 6 show the contour plots of the components of stress and electric displacement around the elliptical void with $\zeta = \pi/4$ and $a/b = 2$ subjected to mechanical and electrical loadings respectively and modeled using single TLG grain. These figures only show the region around the void.

5.2. Evaluation of the material properties of porous piezoelectric materials

In this subsection, we determine the material properties of a porous PZT-4 ceramic as a function of porosity volume fraction using different TLG samples. The material properties of non-porous PZT-4 are listed in Table 2 (denoted TLG-4(2)). Three computational models, shown in Fig. 7, are used to calculate the effective properties of porous PZT-4: C_{11}^{eff}, C_{33}^{eff}, C_{13}^{eff}, e_{31}^{eff}, e_{33}^{eff} and h_{33}^{eff}.

The first model ensures that $\varepsilon_{33} = 0$ and $E_3 = 0$, and is used to calculate C_{11}^{eff} and C_{13}^{eff} as:

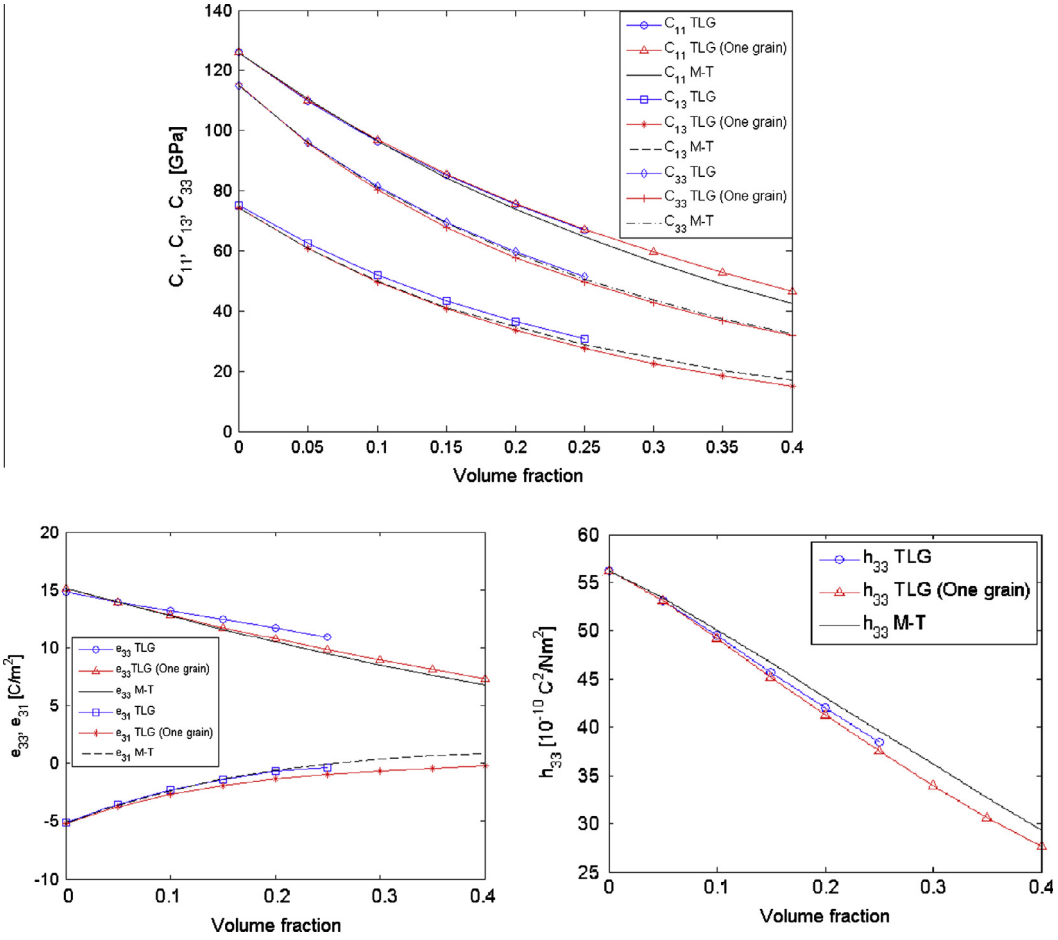

Fig. 9. Predictions of the effective piezoelectric material properties of PZT-4 as a function of porosity volume fraction.

$$C_{11}^{eff} = \frac{\sigma_{11}}{\varepsilon_{11}} = \frac{\int_{x_1=L} t_1 \cdot ds/W}{\bar{u}_1/L}, \quad C_{13}^{eff} = \frac{\sigma_{33}}{\varepsilon_{11}} = \frac{\int_{x_3=W} t_3 \cdot ds/L}{\bar{u}_1/L} \tag{68}$$

The second model ensures that $\varepsilon_{11} = 0$ and $E_3 = 0$, and is used to calculate C_{33}^{eff}, and C_{13}^{eff} as:

$$C_{33}^{eff} = \frac{\sigma_{33}}{\varepsilon_{33}} = \frac{\int_{x_3=W} t_3 \cdot ds/L}{\bar{u}_3/W}, \quad C_{13}^{eff} = \frac{\sigma_{11}}{\varepsilon_{33}} = \frac{\int_{x_1=L} t_1 \cdot ds/W}{\bar{u}_3/W} \tag{69}$$

Finally, the third model ensures that $\varepsilon_{11} = \varepsilon_{33} = 0$, and is used to calculate $e_{33}^{eff}, e_{13}^{eff}$ and h_{33}^{eff} as:

$$e_{33}^{eff} = -\frac{\sigma_{33}}{E_3} = \frac{\int_{x_3=W} t_3 \cdot ds/L}{\bar{\varphi}/W}, \quad e_{13}^{eff} = -\frac{\sigma_{11}}{E_3} = \frac{\int_{x_1=L} t_1 \cdot ds/W}{\bar{\varphi}/W},$$
$$h_{33}^{eff} = \frac{D_3}{E_3} = \frac{\int_{x_3=W} Q \cdot ds/L}{\bar{\varphi}/W} \tag{70}$$

Two types of representative volume element (RVE) are used here as shown in Fig. 8: (a) a unit cell grain with a circular void (the figure shows the case of VF = 40%), (b) 10 TLG grains with random circular voids (the figure shows the case of VF = 25%). Plane strain assumption is used in this study and the direction of polarization is vertically upward in all grains. Since all grain types give very similar results, the simulations are showing only the results of TLG-Cs grain type. The results are compared with the predictions of Mori–Tanaka model [33,34] presented in [32] for PZT-4.

Fig. 9 shows the predictions of the effective properties of PZT-4 as a function of porosity volume fraction. The results of the RVE with 10 TLG grains extends only to VF = 25%. A constraint was used in this mesh in order to prevent the value of the void radius in any grain from exceeding 80% of the distance between the center of the void and the closest point to it on the grain's outer boundary. The figure shows very good agreement with the predictions of Mori–Tanaka's analytical model.

It should be noted that, with the same number of grains, the results slightly change as the irregular mesh changes because the stiffness matrices depends on the grain shape. Changing the mesh changes the integrands of the stiffness matrices, and the number and locations of the collocation points in TLG-C and TLG-Cs. Increasing the number of grains, the maximum order of Trefftz functions used (without violating the conditions in subsection 4.4), and the number of nodes per side in each grain (i.e., using

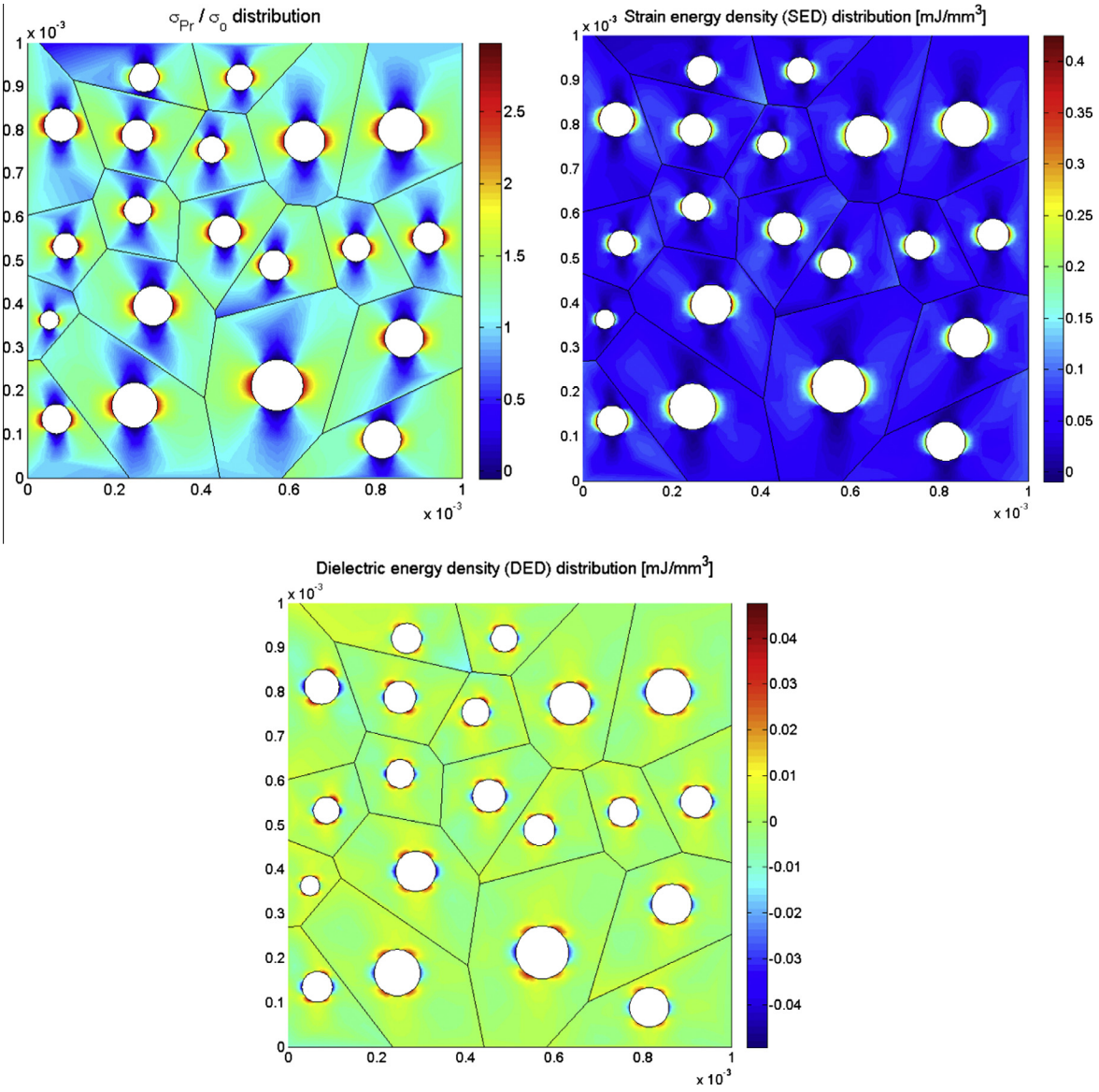

Fig. 10. Porous piezoelectric material under mechanical loading: contour plot for (left) principal stress, (right) strain energy density, (lower) dielectric energy density.

more than two nodes per side) generally has the effect of decreasing the error. Also increasing the number of collocation points in TLG-C and TLG-Cs, increases the accuracy of the solution.

5.3. Damage detection in porous piezoelectric material

We consider porous piezoelectric representative volume element (RVE) composed of 20 porous piezoelectric grains made of PZT-4(1) and polled in the vertical direction. The dimensions of the RVE are $L = W = 1$ mm and the porosity volume fraction is 0.1. The direction of polarization is vertically upward in all grains. Voids in the grains are randomly sized circles. A constraint was used in this mesh in order to prevent the value of the void radius in any grain from exceeding 80% of the distance between the center of the void and the closest point to it on the grain's outer boundary. The lower edge is prevented from motion in the vertical direction while the lower left corner node is electrically grounded and constrained in the horizontal direction. A mechanical loading $\sigma_o = 100$ MPa is applied on the upper edge. The contour plots of the maximum principal stress, the strain energy density (SED) as well as the dielectric energy density are shown in Fig. 10. The results shown here are computed using TLG-C grain type.

As can be seen from the figures, high principal stress and strain energy density concentrations are observed near the cavities, in the direction perpendicular to that of the loading. On the other hand, at the locations near the cavities, in the direction parallel to the loading direction, very low stress values and strain energy density are observed. This gives us an idea about where damage is more likely to initiate and develop in porous piezoelectric materials.

It is also interesting to note that the dielectric energy density concentrates around the voids at angles $\pm 45^{\circ}$ from the mechanical loading direction, and decreases around the voids in the direction perpendicular to that of the loading. As the void gets sharper (b/a ratio is decreased), the variations in the values of the principal stress, as well as the strain and dielectric energy densities on the periphery of the void get larger since the void is approaching the shape of a crack.

6. Conclusions

The proposed TLG grains are capable of modeling porous piezoelectric materials at the micro and meso scales: (a) effective material properties, (b) distribution of all secondary fields, and (c) distribution of strain and dielectric energy densities in the microstructure that allows predicting the locations of damage. Each computational grain has an irregular polygonal shape that resembles the shape of a material grain with arbitrary number of sides and neighboring grains. Each grain also may contain a circular or an arbitrary oriented elliptical void, and may have its own direction of polarization. The grains that used the special solution sets (TLG-BVPs, TLG-Cs and TLG-LSs) are the best in modeling grains with traction-free, charge-free elliptical voids because of their simplicity and efficiency. However these grain formulations need to be modified for other void boundary condition cases such as grains with inclusions, and will be presented in future papers. On the other hand, TLG-C and TLG-LS are more expensive but could be extended to other cases by enforcing the void/inclusion boundary conditions on the void/inclusion periphery. All grain types except TLG-BVP have the advantage of guaranteed stability since Lagrangian multipliers are not involved in their formulations (TLG: Trefftz-Lekhnitskii Grains, BVP: Boundary Variational Principle, C: Collocation, LS: Least Squares, s: Special solution set).

Acknowledgments

This research is supported by the Mechanics Section, Vehicle Technology Division, of the US Army Research Labs, under a collaborative research agreement with UCI. The second author expresses his thanks to the King Abdulaziz University of Saudi Arabia, where he is appointed as a Distinguished Adjunct Professor of Multidisciplinary Engineering & Computer Science. We are also grateful to Dr. Jeffrey Fong of the US National Institute of Standards and Technology (NIST), Gaithersburg, MD, for his critical comments.

References

[1] J.F. Li, K. Takagi, M. Ono, W. Pan, R. Watanabe, A. Almajid, J. Am. Ceram. Soc. 86 (2003) 1094–1098.
[2] D.R. Jin, Z.Y. Meng, F. Zhou, Mater. Sci. Eng. B 99 (2003) 83–87.
[3] J.F. Li, K. Takagi, N. Terakubo, R. Watanabe, Appl. Phys. Lett. 79 (2001) 2441–2443.
[4] K.A. Klicker, J.V. Biggers, R.E. Newnham, J. Am. Ceram. Soc. 64 (1981) 5–9.
[5] B.P. Kumar, H.H. Kumar, D.K. Kharat, Sci. Eng. B 127 (2006) 130–133.
[6] H. Sosa, Int. J. Solids Struct. 28 (4) (1991) 491–505.
[7] X.L. Xu, R.K.N.D. Rajapakse, Acta Mater. 47 (1999) 1735–1747.
[8] M.Y. Chung, T.C.T. Ting, Int. J. Solids Struct. 33 (1996) 3343–3361.
[9] P. Lu, F.W. Williams, Int. J. Solids Struct. 35 (1998) 651–664.
[10] S.G. Lekhnitskii, Anisotropic Plates, Gordon and Breach, Science Publishers, New York, 1968.
[11] A.N. Stroh, Phil. Mag. 3 (1958) 625–639.
[12] L. Dong, S.N. Atluri, CMES: Comput. Model. Eng. Sci. 83 (2) (2012) 183–219.
[13] L. Dong, S.N. Atluri, CMC: Comput. Mater. Continua 29 (2) (2012) 169–211.
[14] L. Dong, S.N. Atluri, CMC: Comput. Mater. Continua 30 (1) (2012) 39–82.
[15] L. Dong, S.N. Atluri, CMES: Comput. Model. Eng. Sci. 89 (5) (2012) 417–458.
[16] L. Dong, S.N. Atluri, CMC: Comput. Mater. Continua 33 (2) (2013) 111–154.
[17] L. Dong, S.N. Atluri, CMES: Comput. Model. Eng. Sci. 90 (2) (2013) 91–146.
[18] L. Dong, S.N. Atluri, CMES: Comput. Model. Eng. Sci. 90 (5) (2013) 379–413.
[19] H. Wang, Q.H. Qin, Acta Mech. 223 (2012) 1323–1340.
[20] X.W. Wang, Y. Zhou, W.L. Zhou, Int. J. Solids Struct. 41 (2004) 7111–7128.
[21] C. Cao, A. Yu, Q.H. Qin, Acta Mech. 224 (2013) 41–61.
[22] X.L. Xu, R.K.N.D. Rajapakse, Composites: Part B (1998) 655–669.
[23] L. Dong, S.N. Atluri, CMES: Comput. Model. Eng. Sci. 85 (1) (2012) 1–43.
[24] N. Sheng, K.Y. Sze, Y.K. Cheung, Int. J. Numer. Methods Eng. 65 (2006) 2113–2138.
[25] P.L. Bishay, S.N. Atluri, CMC: Comput. Model. Eng. Sci. 33 (1) (2013) 19–62.
[26] L. Dong, S.N. Atluri, CMC: Comput. Mater. Continua 24 (1) (2011) 61–104.
[27] P.L. Bishay, S.N. Atluri, CMES: Comput. Model. Eng. Sci. 84 (1) (2012) 41–98.
[28] S.G. Lekhnitskii, Theory of Elasticity of an Anisotropic Body, Mir Publishers, Moscow, 1981.
[29] J.S. Domingues, A. Portela, P.M.S.T. Castro, Eng. Fract. Mech. 64 (1999) 67–86.
[30] I. Babuska, Numer. Math. 20 (3) (1973) 179–192.
[31] F. Brezzi, Anal. Numer. 8 (2) (1974) 129–151.
[32] H. Wang, G. Tan, S. Cen, Z. Yao, Eng. Anal. Bound. Elem. 29 (2005) 636–646.
[33] M. Dunn, M. Taya, J. Am. Ceram. Soc. 76 (7) (1993) 1697–1706.
[34] Y. Mikata, Int. J. Eng. Sci. 38 (2000) 605–641.